Flinders UNIVERSITY
ADELAIDE · SOUTH AUSTRALIA

# Assessment of Managed Aquifer Recharge Impact on Groundwater Using Groundwater Modelling in Dong Khwang, Sakon Nakhon Province, Thailand

By

**Sirilack Duangsong**

*Thesis*
*Submitted to Flinders University*
*for the degree of*

**Master of Science (Groundwater Hydrology)**

College of Science and Engineering
30 May 2025

# TABLE OF CONTENTS

# ABSTRACT

This study evaluates the effectiveness of a Managed Aquifer Recharge (MAR) system implemented in Dong Khwang village, Sakon Nakhon Province, Northeastern Thailand, as a response to the growing challenge of water scarcity affected by climate change. By employing field observations, hydrogeological data, and numerical groundwater modelling using MODFLOW via ModelMuse, the research simulates groundwater conditions both with and without the MAR system over a ten-year period. The study area is characterised by unconfined and unconsolidated aquifers, which have low permeability, along with variable rainfall and high evapotranspiration rates, which limit natural recharge. Model calibration, which involved manual parameter adjustment, achieved a root mean square residual (RMSR) of less than 1.3 m, confirming model reliability. Results indicate that the MAR system significantly enhanced the groundwater resources, reversing the future decreasing resources (-0.39 $Mm^3$) to an increase of 0.88 $Mm^3$ by 2034. This represents an additional 1.26 $Mm^3$ compared to natural conditions, with the maximum increase in water level reaching 0.57 m. Additionally, 12,310 $m^3$/year of water is now available to support the domestic consumption needs of 684 residents, and more than 72,190 $m^3$/year is still available for agriculture during the dry season. Furthermore, the MAR has influenced groundwater flow across an area of approximately 1.3 $km^2$, with water travelling up to 2.7 km from the system by 2034. These findings confirm that MAR represents a viable solution for sustaining groundwater levels in drought-prone regions and support its integration into long-term water resource planning in Thailand.

# DECLARATION

I certify that this thesis does not incorporate without acknowledgment any material previously submitted for a degree or diploma in any university; and that to the best of my knowledge and belief it does not contain any material previously published or written by another person except where due reference is made in the text.

Signed Sirilack Duangsong

Date 30 May 2025

# ACKNOWLEDGEMENTS

I would like to express my sincere gratitude to the Department of Groundwater Resources and the Groundwater Development Fund of Thailand for recognising the importance of enhancing the skills and capabilities of their personnel. I am honoured to have been awarded a scholarship that enables me to deepen my understanding of groundwater at Flinders University.

I would like to express my sincere gratitude to my supervisor, Professor Okke Batelaan, for his unwavering support and guidance throughout my research project. His expertise, insights, and constructive feedback have been crucial to the successful completion of this study. I also wish to acknowledge Dr. Kriangsak Pirarai and Miss Ocpasorn Occarach for their invaluable assistance in providing essential data for this research. Additionally, I would like to extend my thanks to Dr. Peter Dillon for inspiring me to pursue my studies at Flinders University.

Lastly, I would like to express my appreciation to my colleagues, friends, and family for their steadfast support and encouragement during challenging times. I am deeply grateful for your contributions, which have been instrumental in my journey. Ultimately, I wish to commend my own perseverance and determination in seeing this research endeavour through to its conclusion.

# LIST OF FIGURES

# LIST OF TABLES

# 1. INTRODUCTION

## 1.1 Setting

Global climate change brings urgent challenges and impacts on natural systems, economies, and societies worldwide. For example, rising temperatures and warming have led to more frequent and severe heat waves, droughts, and tropical storms. These events threaten food security, disrupt ecosystems, and lead to significant human and economic losses (World Resources Institute, 2025).

Climate variability and change affect groundwater systems directly by influencing recharge rates and indirectly by altering groundwater usage patterns (Taylor et al., 2013). Direct impact, changes in precipitation patterns, and increased temperatures will affect groundwater recharge rates and the depths of groundwater tables due to higher evapotranspiration (Bovolo et al., 2009). The indirect impact, the influence of humans, has also significantly affected the terrestrial water system through irrigation needs, with these impacts often exceeding the direct effects of climate on water recharge (Taylor et al., 2013).

Climate change also significantly impacts Thailand, disrupting agricultural systems, depleting water resources, and damaging coastal ecosystems, resulting in economic losses. Raised temperatures and unpredictable rainfall reduce crop yields, particularly for rice, while also causing risks to food security (East Asia Forum, 2020).

Sakon Nakon Province is located in Northeast Thailand, an important agricultural region known for growing jasmine rice and other varieties. However, the area faces several challenges, including a lack of water sources and irrigation systems, arid soil conditions, and low fertility. Additionally, it is often far from reliable water sources, and the changing weather, frequent droughts, and natural disasters contribute to ongoing difficulties for farmers (Phuprakit, 2024). As a result, groundwater has been used to supply water for agriculture. This causes a decline in groundwater levels (Department of Groundwater Resources, 2022).

According to Dillon (2021), Managed Aquifer Recharge systems (MAR) are used in more than ten countries to adapt to climate change and ensure that groundwater remains available for the long term. MAR helps improve water security, making it an important part of managing water resources.

Thailand is one of many countries that apply MAR to infill surface water into groundwater. In 2021, the Department of Groundwater Resources (DGR), Thailand, conducted an experimental project to recharge groundwater aquifers with surface water in Dong Khwang village, Sakon Nakhon Province, in Northeastern Thailand.

## 1.2 Objective

The DGR intends to address the water shortage that local residents experience during the summer by establishing a MAR site. This site will facilitate surface water infiltration to enhance the groundwater resources in the unconfined aquifer. However, the observation wells installed to monitor the water level are located very close to the MAR system. As a result, the water level in the observation wells varies in relation to the water level in the MAR system, rather than the water table. Therefore, the water level in the observation wells did not show a significant difference before and after the construction of the MAR system. Consequently, the DGR requires additional tools to evaluate future changes in groundwater conditions, such as water levels and the quantity of water stored in the aquifer, which are essential for effective water management planning.

This research is focused on assessing the results of the MAR system established by the DGR. This research builds on previous studies and readily available information to create both a conceptual model and a numerical groundwater flow model for the study area. The numerical model was developed utilising ModelMuse, a graphical user interface for MODFLOW, which simulates the distribution of hydraulic heads in transient conditions, evaluates water balances, and determines the travel times of water particles. Additionally, the study will forecast water levels under different scenarios, including with and without the construction of the MAR system. The analysis will focus on water levels, recharge rates, and the effects on aquifers following the construction of a MAR system. The model results were thoroughly analysed to enhance our understanding of groundwater resources. This analysis encompasses both historical data and future projections.

This study aims (i) to simulate the groundwater heads and flows using groundwater modelling, both with and without the construction of the MAR system, (ii) to estimate water levels in different scenarios, (iii) to compare the hydraulic head of the two scenarios, and (iv) to estimate the amount of water contributed to the aquifer.

# 2. BACKGROUND AND STUDY AREA

## 2.1 Background

The study area is in Ban Dong Kwang, Dong Mafai Subdistrict, Mueang Sakon Nakhon District, Sakon Nakhon Province, which is located in the Nam Kam Basin. According to the DGR study (Department of Groundwater Resources, 2021), this study area is moderately suitable for groundwater recharge because the highly suitable areas are private land. According to the Department of Land (2019), when the state needs to acquire land for essential public utilities, national defence, natural resource acquisition, or other public benefits, the landowner must provide the land to the public. The suitable areas for MAR are shown in Figure 1.

Figure removed due to copyright restriction.

**Figure 1** Managed Aquifer Recharge suitability map for the Nam Kam Basin.

The Department of Groundwater Resources (2021) developed the map (Figure 1) by analysing various physical data, including geological, geomorphological, soil series, soil infiltration rate, and slope information, utilising a Geographic Information System (GIS) to create the base map. Subsequently, field data were gathered, encompassing water table levels, groundwater extraction, water scarcity, soil salinity, sources of contamination, groundwater flow direction, water quality, and the awareness and understanding of the local population in the study area. This information was then used to create the MAR suitability map.

## 2.2 Population

According to the latest population data from the Official Statistics Registration Systems (Department of Provincial Administration, 2024), the study area has a total of 236 households and a population of 684 people. This population consists of 342 men and 342 women.

## 2.3 Land Use

As shown in Figure 2, agricultural activities, including active paddy fields, cassava, para rubber, oil palm, eucalyptus, teak, bur-flower tree, longan, and livestock, account for the majority of land use, 97.08% of the total area. Following this are forested regions at 1.41%, community and residential areas at 0.95%, other land classifications at 0.48%, and water sources at a minimal 0.08%.

## 2.4 Topography

The study area in the south is situated in the vicinity of the Phu Phan Mountain range, which ranges in elevation from 200 to 600 meters above mean sea level. In the northeast, the land gradually slopes to form a plateau at an elevation of approximately 170-198 meters above mean sea level (Figure 3).

## 2.5 Water use

The Department of Provincial Administration (2024) reports that the study area has a total population of 684 people. Each person uses an average of 3.6 $m^3$ of water per month (Statista, 2021), resulting in a total monthly water consumption of 2,462 $m^3$.

Figure removed due to copyright restriction.

**Figure 2** Land use in the study area.

Figure removed due to copyright restriction.

**Figure 3** Location map of the study area (Sakon Nakhon Province).

## 2.6 Geology

The study area is located in the Khorat Plateau, distinguished by the Phu Phan Mountain range, which is formed by an anticlinorium structure oriented in a northwest-southeast direction. This geological configuration results in the northern region developing the Udon Thani-Sakon Nakhon sub-basin. In contrast, the southern region comprises the Khorat-Ubon Ratchathani sub-basin (Department of Mineral Resources, 2007). Sakon Nakhon Province is positioned within the Udon-Sakon Nakhon sub-basin. The geological composition of the study area is primarily characterised by the Khorat Group, which is identified as a Mesozoic red bed deposited in non-marine environments. This group predominantly consists of siltstone, sandstone, mudstone, and conglomerate from the late Triassic to the Cretaceous-Tertiary periods. It is situated above a surface formed by the weathering of Upper Paleozoic rocks. Figure 4 shows the stratigraphy organised in a sequence from the oldest to the youngest.

### 2.6.1 The Mesozoic era

The Mesozoic era includes the Khorat Group, which is discontinuously layered over older rocks, with conglomerate layers at the base. Currently, the Khorat Group is divided into nine rock formations (Department of Mineral Resources, 2011), namely Huai Hin Lat, Nam Phong, Phu Kradueng, Phra Wihan, Sao Khrua, Phu Phan, Khok Kruat, Maha Sarakham, and Phu Thok

Formation. However, only four rock formations were identified in the study area. The Cretaceous rocks are arranged from oldest to youngest as follows:

(1) The Sao Khua Formation (Ksk) consists of siltstone and sandstone, reddish brown, purple, and red, calcareous, with abundant calcrete and some silcrete horizons.

(2) The Phu Phan Formation (Kpp) consists of sandstone, grey, greenish grey, brown, commonly pebbly and cross-bedded, thick-bedded; siltstone and conglomeratic sandstone with pebbles of quartz, chert, jasper, and igneous rocks.

(3) The Khok Kruat Rock Formation (Kkk) consists of siltstone and sandstone, brownish red and red, calcareous, claystone and conglomerate, with calcrete horizons.

(4) The Maha Sarakham Formation (KTms) consists of siltstone, reddish brown, pale red, claystone, sandstone, and frequent rock salt, potash, gypsum, and anhydrite.

### 2.6.2 Quaternary Unconsolidated Sediments (Qa)

Quaternary unconsolidated sediments are formed through the transport of rocks, gravel, sand, and soil by water, resulting in accumulation in areas located at a distance from riverbanks, particularly near elevated terrains. The composition includes gravel, sand, silt, and clay, which gather along river channels, embankments, and floodplains.

Figure removed due to copyright restriction.

**Figure 4** Geology of the study area (Department of Mineral Resources, 2007).

## 2.7 Hydrogeology

There are two main aquifers, including a consolidated aquifer and an unconsolidated aquifer, as shown in Figure 5.

### 2.7.1 Consolidated aquifer

1) The Middle Khorat Unit comprises the Phu Phan and the Sao Khua Formation, including siltstone, sandstone, and gravel. These geological formations are characterised by their density, hardness, and resistance to erosion, resulting in the formation of cliffs or plateaus. The layers are generally thick and exhibit few fractures (Department of Mineral Resources, 2007). As a result, wells drilled in these units typically yield a limited water supply. However, deep fractures may lead to the discovery of flowing artesian wells in specific locations. Furthermore, if the Sao Khua Formation consists of shale formed from the solidification of lake sediments, it is possible to obtain water from the fractures within this hard shale (Department of Mineral Resources, 2007).

2) The Upper Khorat Unit comprises the Mahasarakham and Khok Kruat Formations. The Mahasarakham Formation is primarily mudstone or claystone and typically yields saline water. However, the water quality can range from poor to moderate in shallow areas or low hills. In contrast, the Khok Kruat Formation contains good-quality groundwater stored in the fractures of the rock layers, providing a yield of approximately 5 to 10 cubic meters per hour.

### 2.7.2 The unconsolidated Aquifer

The study area comprises alluvium (Qa) with a thickness estimated to be between 10 and 15 meters. The hydraulic properties of this aquifer can be assessed using data obtained from pumping tests (Trinet et al., 2008), including both constant rate pumping tests and slug tests. The transmissivity ranges from 3.19 to 21.33 $m^2$/day, while the water storage coefficient varies between 0.006 and 0.10 (Trinet et al., 2008). The hydraulic conductivity of the alluvium ranges from 0.012 to 2.88 m/day (Land Development Department 2016).

Figure removed due to copyright restriction.

**Figure 5** Hydrogeology of the study area (Department of Groundwater Resources, 2012).

## 2.8 Hydrostratigraphy

The investigation of soil and rock samples, in conjunction with the results from geophysical surveys using 2D electrical resistivity measurements and geophysical logging, has provided valuable insights into the subsurface composition of the study area. The analysis indicates that geology comprises sedimentary and hard rock layers. Within the 0 to 22 meters depth range, alternating layers of sandy clay and clay (Qa) were identified. The Khok Kruat Formation (Kkk) was also observed from depths of 22 meters (Department of Groundwater Resources, 2022), shown in Figure 6. Notably, a coarse-grained groundwater layer was located at depths ranging from 4 to 12 meters.




**Figure 6** Geological cross-section of the study area (modified from Department of Groundwater Resources, 2022).

## 2.9 Precipitation

Precipitation data were collected from Sakhon Nakhon Station, station number 356201. The annual rainfall in Sakon Nakhon Province over the past twenty years (2005–2024) has varied from 1,200 to 2,400 millimetres (mm) per year (Meteorological Department, 2024). The rainy season, from June to October, typically experiences rainfall ranging from less than 10 mm to 800 mm per month. During the summer months of March to May, moderate rainfall occurs, with monthly totals ranging from less than 10 mm to 400 mm. From November to February, light rainfall is recorded in winter, ranging from 0 to 130 mm per month. The highest levels of rainfall are usually observed in July and August, as shown in Table 1. The trend line illustrates a decrease in precipitation rates from 2005 to 2024, as represented in Figure 7.

## 2.10 Evapotranspiration (ET)

The evaporation data was collected from the Sakhon Nakhon Station, station number 356201. The data were then used to estimate reference evapotranspiration ($ET_0$), which was calculated using the FAO Penman-Monteith equation and converted to actual evapotranspiration (ET) using Crop Coefficients (Kc) by the Meteorological Department. This method is internationally recognised as the standard method for estimating evapotranspiration from a reference crop (Allen et al., 1998).

The evapotranspiration in Sakon Nakhon Province over the past twenty years (2005–2024) ranges between 1,300 and 1,500 mm per year (Meteorological Department, 2024). The summer typically shows an evapotranspiration rate between 80 and 200 mm per month. During the rainy season, the monthly totals range from 80 to 150 mm. In winter, it is recorded ranging from 50 to 130 mm. The highest evapotranspiration rate is typically observed in April, as shown in Table 2. The trend line shows a decline in evapotranspiration rates from 2005 to 2024, as depicted in Figure 8.

**Table 1** Monthly, total, and average rainfall in mm over the past twenty years (2005-2024).

| Month / Year | Jan | Feb | Mar | Apr | May | Jun | Jul | Aug | Sep | Oct | Nov | Dec | Total | Average |
|---|---|---|---|---|---|---|---|---|---|---|---|---|---|---|
| **2005** | 0.5 | 0.0 | 21.0 | 77.1 | 274.4 | 296.6 | 482.3 | 334.7 | 323.3 | 13.2 | 6.7 | 0.0 | 1829.8 | 152.5 |
| **2006** | 0.0 | 12.0 | 33.4 | 107.3 | 210.9 | 165.5 | 358.5 | 274.0 | 91.5 | 218.8 | 130.3 | 0.0 | 1602.2 | 133.5 |
| **2007** | 0.0 | 39.0 | 67.1 | 38.8 | 219.1 | 246.5 | 172.3 | 498.0 | 307.4 | 228.1 | 7.1 | 0.0 | 1823.4 | 151.9 |
| **2008** | 7.3 | 7.7 | 126.6 | 188.9 | 228.3 | 293.6 | 401.4 | 336.9 | 395.5 | 113.7 | 35.3 | 6.8 | 2142.0 | 178.5 |
| **2009** | 0.3 | 0.0 | 89.1 | 109.3 | 246.0 | 213.4 | 388.3 | 257.3 | 98.5 | 21.4 | 0.5 | 16.3 | 1440.4 | 120.0 |
| **2010** | 54.9 | 38.7 | 25.3 | 74.4 | 133.0 | 193.1 | 191.7 | 397.8 | 250.8 | 87.2 | 0.0 | 3.0 | 1449.9 | 120.8 |
| **2011** | 0.0 | 14.8 | 21.5 | 66.0 | 327.4 | 257.1 | 323.9 | 458.1 | 220.2 | 200.8 | 2.8 | 0.0 | 1892.6 | 157.7 |
| **2012** | 30.4 | 6.0 | 58.7 | 401.9 | 221.2 | 230.1 | 272.7 | 321.3 | 163.8 | 13.1 | 21.8 | 0.0 | 1741.0 | 145.1 |
| **2013** | 0.5 | 0.6 | 22.5 | 85.5 | 331.2 | 290.3 | 615.5 | 263.2 | 349.0 | 51.9 | 0.4 | 33.7 | 2044.3 | 170.4 |
| **2014** | 0.0 | 0.0 | 18.0 | 101.1 | 137.9 | 325.6 | 520.9 | 227.2 | 284.5 | 50.6 | 14.1 | 0.2 | 1680.1 | 140.0 |
| **2015** | 3.2 | 91.8 | 77.7 | 26.3 | 223.1 | 105.8 | 408.6 | 258.9 | 121.3 | 82.5 | 40.5 | 0.2 | 1439.9 | 120.0 |
| **2016** | 14.6 | 0.0 | 2.8 | 75.8 | 89.2 | 342.3 | 207.0 | 264.7 | 280.2 | 46.2 | 22.9 | 3.6 | 1349.3 | 112.4 |
| **2017** | 2.0 | 15.4 | 191.6 | 89.5 | 301.1 | 455.8 | 796.6 | 248.4 | 203.4 | 108.7 | 1.0 | 9.4 | 2422.9 | 201.9 |
| **2018** | 0.0 | 67.1 | 41.9 | 52.0 | 133.4 | 318.3 | 559.4 | 224.5 | 160.6 | 2.2 | 0.0 | 0.6 | 1560.0 | 130.0 |
| **2019** | 0.0 | 19.7 | 12.9 | 64.0 | 206.5 | 102.1 | 226.5 | 411.2 | 161.0 | 7.5 | 1.6 | 0.0 | 1213.0 | 101.1 |
| **2020** | 20.9 | 0.0 | 120.2 | 29.3 | 197.8 | 146.5 | 228.7 | 268.5 | 126.8 | 144.7 | 1.2 | 0.0 | 1284.6 | 107.1 |
| **2021** | 0.0 | 21.6 | 84.3 | 153.8 | 91.2 | 276.5 | 284.2 | 158.4 | 182.6 | 175.8 | 0.3 | 0.0 | 1428.7 | 119.1 |
| **2022** | 1.6 | 38.8 | 62.8 | 25.8 | 250.2 | 122.2 | 223.7 | 174.1 | 232.9 | 49.9 | 22.9 | 0.0 | 1204.9 | 100.4 |
| **2023** | 18.7 | 6.8 | 1.5 | 35.8 | 109.5 | 390.2 | 423.0 | 326.2 | 573.4 | 83.2 | 0.0 | 0.0 | 1968.3 | 164.0 |
| **2024** | 0.2 | 3.2 | 14.0 | 29.0 | 184.5 | 145.0 | 268.1 | 441.8 | 328.1 | 10.2 | 0.0 | 0.0 | 1424.1 | 142.4 |

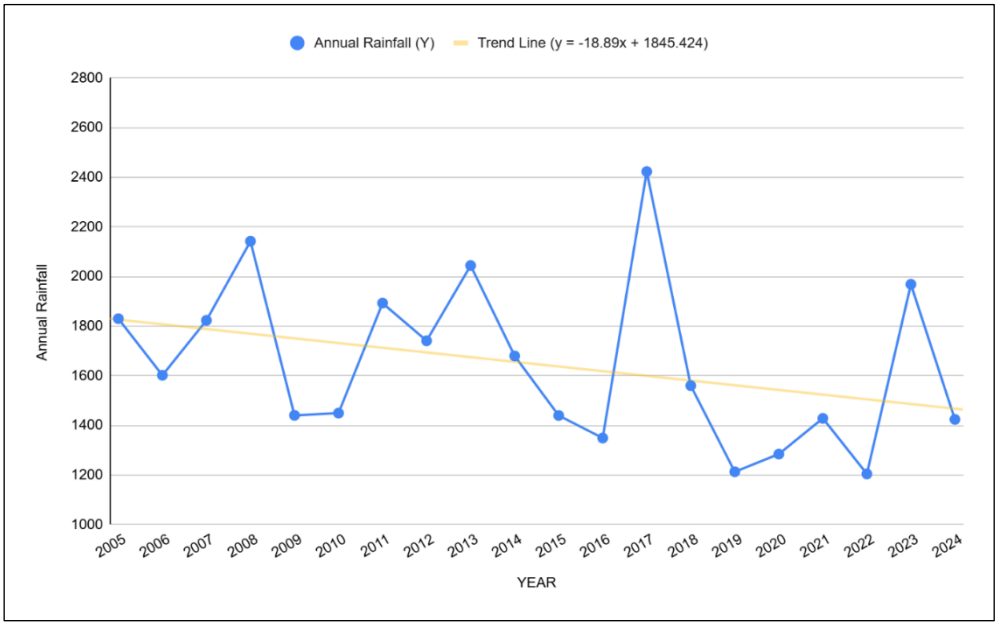


**Figure 7** Annual rainfall data collected from Sakhon Nakhon Station, station number 356201, over twenty years, and including the trend line.

**Table 2** Monthly and average evapotranspiration rate in mm over the past twenty years (2005-2024).

| Month / Year | Jan | Feb | Mar | Apr | May | Jun | Jul | Aug | Sep | Oct | Nov | Dec | Total | Average |
|---|---|---|---|---|---|---|---|---|---|---|---|---|---|---|
| **2005** | 116.9 | 137.2 | 160.5 | 153.1 | 139.3 | 108.8 | 109.6 | 82.7 | 101.4 | 133.1 | 112.5 | 117.5 | 1472.6 | 122.7 |
| **2006** | 132.7 | 137.1 | 156.7 | 141.8 | 133.5 | 126.2 | 103.4 | 105 | 124.5 | 116.6 | 119.9 | 113.8 | 1511.2 | 125.9 |
| **2007** | 129.8 | 118.5 | 143.3 | 181.8 | 161.3 | 126.2 | 125 | 103.3 | 103.1 | 107.5 | 113 | 115.1 | 1527.9 | 127.3 |
| **2008** | 116.6 | 120.4 | 157 | 154.2 | 122 | 101.1 | 106.8 | 94.2 | 100.9 | 114.9 | 119.5 | 100.4 | 1408 | 117.3 |
| **2009** | 114.5 | 130.5 | 151.6 | 159.3 | 144 | 126.5 | 108.6 | 110.2 | 112.4 | 125.4 | 124.3 | 108 | 1515.3 | 126.3 |
| **2010** | 106.3 | 107.4 | 163.7 | 174.5 | 152.4 | 115.3 | 135 | 92.7 | 97.7 | 114.9 | 114.1 | 110.1 | 1484.1 | 123.7 |
| **2011** | 127.4 | 118.8 | 153.9 | 163.7 | 131.9 | 125.8 | 109.5 | 105.5 | 95.1 | 103.9 | 120.5 | 110.2 | 1466.2 | 122.2 |
| **2012** | 107.7 | 124.3 | 148.1 | 121.9 | 130.1 | 127.1 | 125 | 114.8 | 118.8 | 142.9 | 123.1 | 123 | 1506.8 | 125.6 |
| **2013** | 115.8 | 137 | 168.5 | 181.5 | 142.5 | 107.4 | 94.8 | 112.3 | 98.8 | 125.3 | 113.1 | 91 | 1488 | 124 |
| **2014** | 99.8 | 116.1 | 158.5 | 147.7 | 149.7 | 124.6 | 84.6 | 107.6 | 104.2 | 126.8 | 113.4 | 106.3 | 1439.3 | 119.9 |
| **2015** | 101.8 | 116.4 | 128.1 | 170.6 | 165.3 | 150.8 | 111.6 | 125.6 | 108.5 | 123.4 | 119.5 | 115 | 1536.6 | 128 |
| **2016** | 97 | 141.4 | 178.3 | 190.4 | 160.7 | 126.8 | 124.9 | 116.4 | 101.4 | 114.9 | 107.1 | 104.6 | 1563.9 | 130.3 |
| **2017** | 119 | 132.1 | 126.5 | 127.6 | 121.5 | 113 | 72.1 | 120.3 | 106.9 | 115.5 | 114.2 | 105 | 1373.7 | 114.5 |
| **2018** | 116.8 | 115.5 | 141 | 149.8 | 133.7 | 110.5 | 113.9 | 91.8 | 133.9 | 145.5 | 107.8 | 118.5 | 1418.7 | 118.2 |
| **2019** | 127.6 | 121.2 | 173.5 | 172.1 | 132.2 | 131.3 | 127.8 | 112.8 | 128.2 | 145.3 | 114 | 108.1 | 1594.1 | 132.8 |
| **2020** | 119.5 | 137.8 | 139.1 | 171.2 | 163.7 | 124.9 | 134.7 | 98.7 | 105.4 | 93.2 | 103 | 100.8 | 1492 | 124.3 |
| **2021** | 106.9 | 121.8 | 141.2 | 140.3 | 151.2 | 132.6 | 123.9 | 132.7 | 106.1 | 99.3 | 116.1 | 99.4 | 1471.5 | 122.6 |
| **2022** | 107.5 | 107.5 | 132.9 | 139.9 | 106.6 | 122.6 | 120.4 | 109.4 | 103 | 118.4 | 107.7 | 110.4 | 1386.3 | 115.5 |
| **2023** | 103.5 | 121.8 | 167.3 | 179.8 | 175.2 | 119.2 | 107.9 | 106.1 | 91.8 | 121.1 | 114.2 | 109.9 | 1517.8 | 126.5 |
| **2024** | 110.7 | 129.3 | 88 | 198.8 | 157.3 | 113.7 | 101.8 | 104.9 | 30.7 | 120.1 | 116 | 110.3 | 1432.9 | 119.4 |

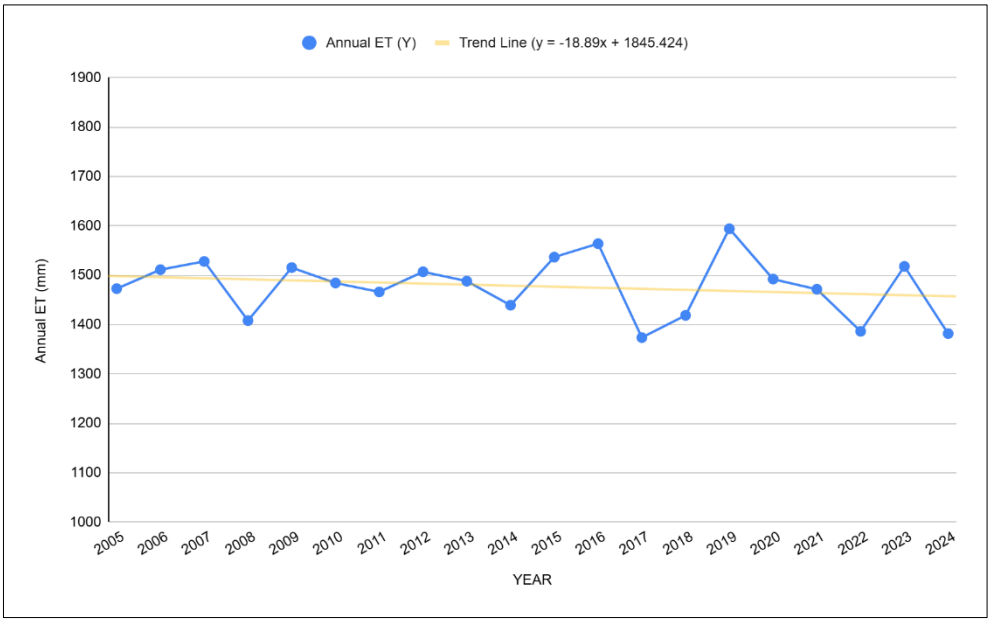


**Figure 8** Annual potential evapotranspiration data collected from Sakhon Nakhon Station, station number 356201, over twenty years and the trend line.

## 2.11 Equipotential lines and flow directions

Groundwater in the study area is influenced by rainfall, reservoirs, creeks, and recharge areas adjacent to the southwest mountains. An analysis was conducted on the equipotential lines derived from groundwater level data collected from 39 shallow groundwater wells in June 2021 (Department of Groundwater Resources, 2021). The point elevations were interpolated into a raster file using the Inverse Distance Weighted (IDW) method. Subsequently, contour lines were generated using the contour tool within the spatial analysis framework. The analysis reveals that groundwater flows from the southwest to the northeast. The equipotential lines located to the west and north of the study area, as well as to the east of the MAR site, indicate a low water level that is influenced by water pumping, as shown in Figure 9.

Figure removed due to copyright restriction.

**Figure 9** Groundwater flow direction in Dong Khwang, Sakon Nakhon Province, in Northeastern Thailand. The equipotential lines derived from groundwater level data collected from 39 shallow wells in June 2021

## 2.12 Construction plan

Before the construction of the MAR system, the study area contained two ponds that were excavated to a depth of approximately 2.5 to 3 meters. These ponds were situated within a layer of fine-grained sediment. The ponds were used to store rainwater. The design and rehabilitation of the ponds made them deeper and larger. The DGR classified one pond as a sediment basin and the other as a reservoir. Water will flow into the sediment basin, where sediment will settle before the water is channelled into the reservoir. From there, it will recharge the aquifer.

The MAR system was constructed, and recharge commenced in December 2021. The sediment basin originally had an area of 3,390 m², which has now increased to 4,000 m², and its depth was 2.5 m, however, it is now 5 m. The reservoir's area was 2,700 m² and has now expanded to 3,200 m², with the depth increasing from 3 m to 5 m. The canal width has increased from 15 m to 18 m, and its depth has grown from 2.45 m to 3 m. Additionally, an inlet and outlet have been constructed to facilitate the flow of water into and out of the sediment basin, and 6 observation wells were also installed to observe groundwater level at the MAR site, as shown in Figure 10.

Figure removed due to copyright restriction.

**Figure 10** MAR construction plan and observation wells (The Department of Groundwater Resources, 2022).

## 2.13 Lithological logging of observation wells

Lithological logging is the systematic recording and analysis of different rock types, minerals, and soil characteristics found in observation wells. This process involves examining physical properties, including colour, texture, and grain size of the sediments. The data collected from lithological logging is essential for evaluating soil layers.

The DGR drilled 6 observation boreholes (Figure 10) and collected samples from each borehole at one-meter intervals. Following this, they conducted electrical logging to assess the soil properties. The interpretation of soil type was derived from the combination of borehole samples and electric logging data, as illustrated in Figure 11.

Figure removed due to copyright restriction.

(a)

Figure removed due to copyright restriction.

(b)

Figure removed due to copyright restriction.

(c)

Figure removed due to copyright restriction.

(d)

Figure removed due to copyright restriction.

(e)

Figure removed due to copyright restriction.

(f)

**Figure 11** Lithological description of the observation wells (Department of Groundwater Resources, 2022). (a) Well No.1, (b) Well No.2, (c) Well No.3, (d) Well No.4, (e) Well No.5, and (f) Well No.6.

## 2.14 Conceptual model

Based on the lithological description of the observation wells, the model can be divided into three layers. The first layer (Qa) ,upper unconfined aquifer, consists of very fine to fine-grained sediments and has a thickness of 4 meters. The second layer (Qa), middle layer, consists of fine to medium-grained sediments with a thickness of 12 meters. The third layer (Kkk), lower layer, is composed of consolidated rock with a thickness of 20-30 meters, as shown in Figure 12.

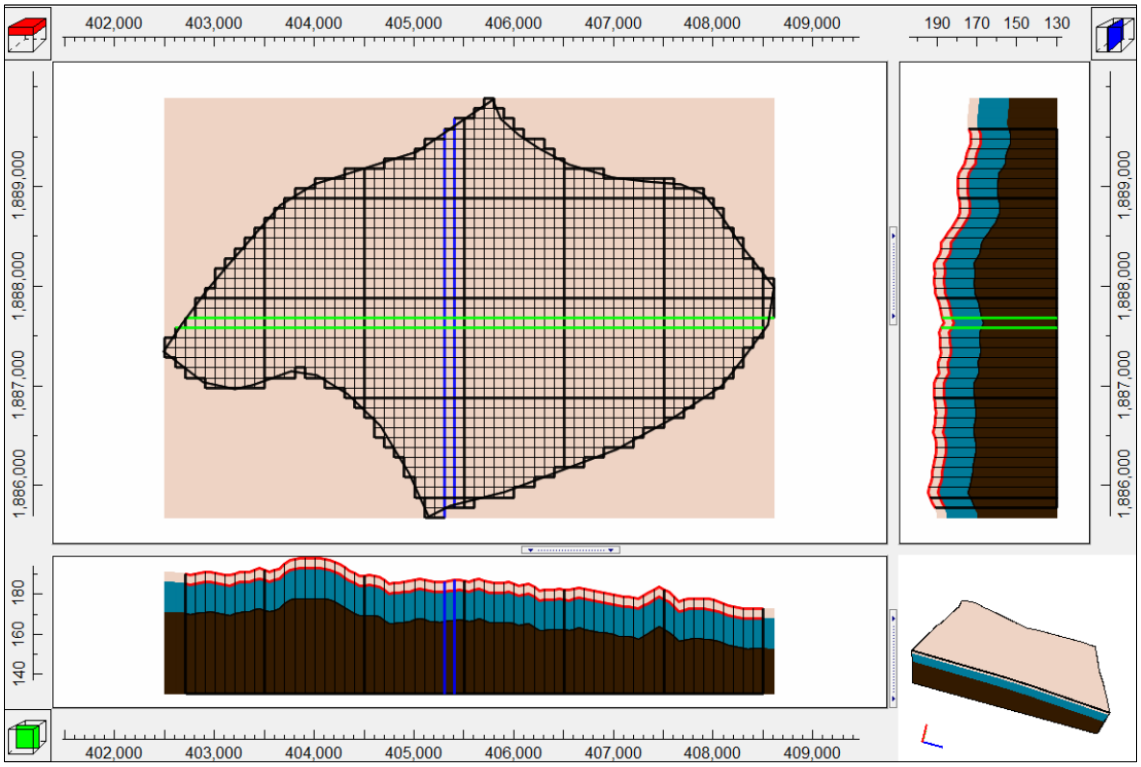


**Figure 12** Conceptual model, which is divided into three layers based on the lithological logging of the six observation wells.

# 3. METHODOLOGY

## 3.1 Model setup

### 3.1.1 Model extent

The model domain covers an area of 14.27 $km^2$, and the MAR system is located in the centre of the domain. The model was constructed with the ModelMuse interface and set up to function in a transient state, with hydraulic conductivities expressed in meters per day (m/d). The model area was divided into 3 layers, utilising grid cells measuring from 20 m to 40 m grid cell resolution, resulting in a total of 151 rows and 202 columns.

### 3.1.2 Boundary conditions

The study area consists of a relatively flat landscape without main rivers, which challenges defining the model's boundaries. Therefore, the boundaries on each side of the model can be set as follows:

**1) The boundaries to the Northeast and Southwest** were defined using the equipotential lines as constant head boundaries. These equipotential lines were created based on the water levels recorded in the shallow groundwater wells within the study area for two periods, **before** and **after** the construction of the MAR system, specifically in June 2021 and June 2022. According to Figure 13, the groundwater level that exhibited the least difference between these two periods was selected as the constant head.

**2) The boundaries of the Northwest and Southeast** were defined using a groundwater flow line as a no-flow boundaries, assuming that the groundwater flows only in directions perpendicular to the equipotential line. The boundary of the model is shown in Figure 13.

Figure removed due to copyright restriction.

**Figure 13** Boundary of the model created from the equipotential lines.

### 3.1.3 Layer distribution

#### 1) Surface elevation (Model Top)

The model top was established using the Digital Elevation Model (DEM) (SRTM Thailand, 2022), which has a pixel size of 30 m x 30 m. However, the grid cell size of the model differs from that of the DEM. As a result, ModelMuse will calculate the elevation value for each grid cell by averaging all the DEM pixels within that grid cell and then assigning this average value to the grid cell. Figure 14 shows the model top elevation after assigning the elevation using the DEM.

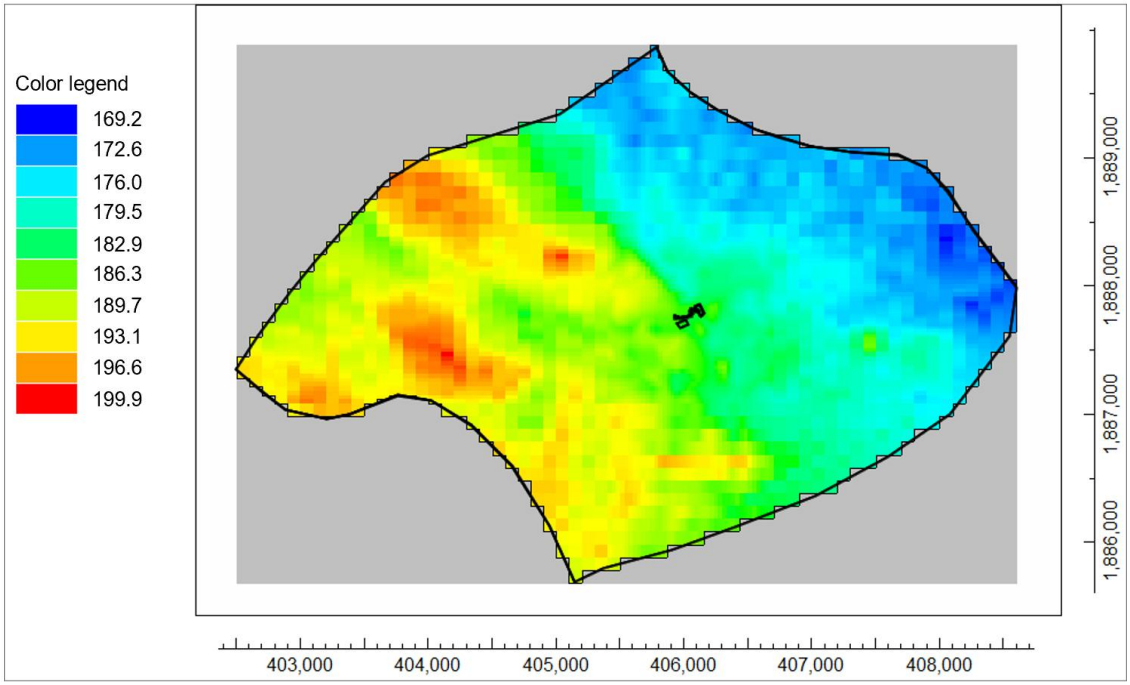


**Figure 14** Model Top elevation (meters above mean sea level (m.a.s.l.)).

#### 2) Layer definition

Based on the borehole data, the model was established with three layers as follows:

1. The upper unconfined aquifer is primarily composed of clayey sand, characterised by a mixture of very fine to fine sand particles. This aquifer layer has an approximate thickness of 4 meters.
2. The middle layer consists of clayey sand, which is composed of fine to medium-grained sand. This layer has an approximate thickness of 12 meters.
3. The lower layer, which is below a depth of 16 meters, is composed of Shale.

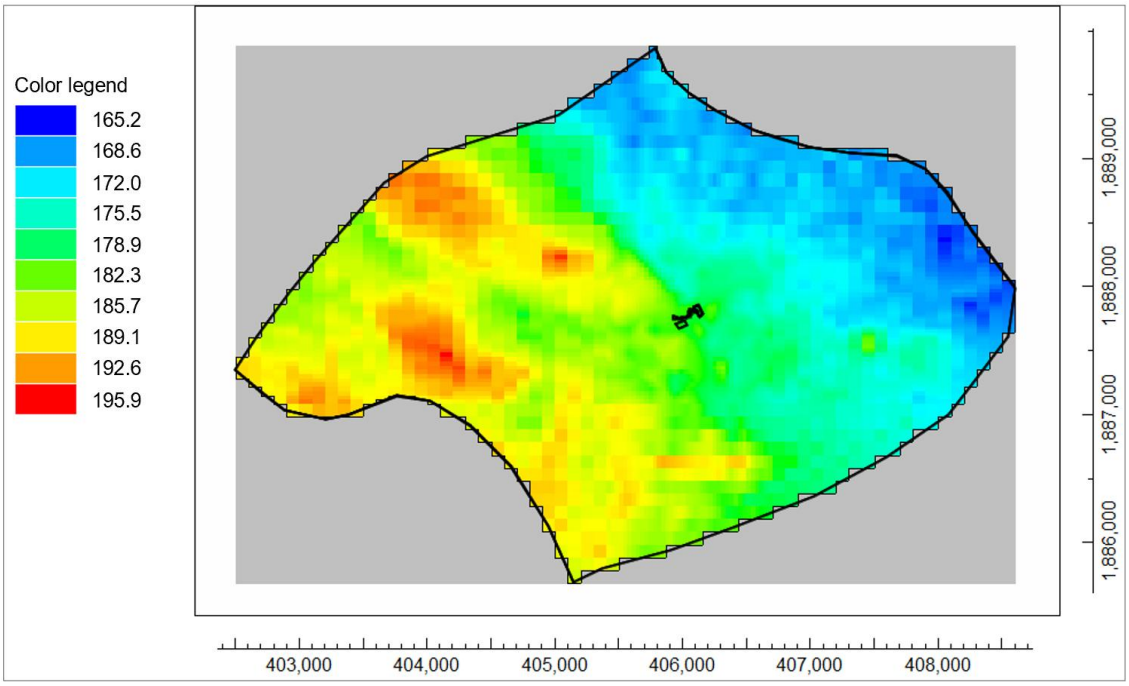


**Figure 15** Top middle layer elevation (m.a.s.l.).

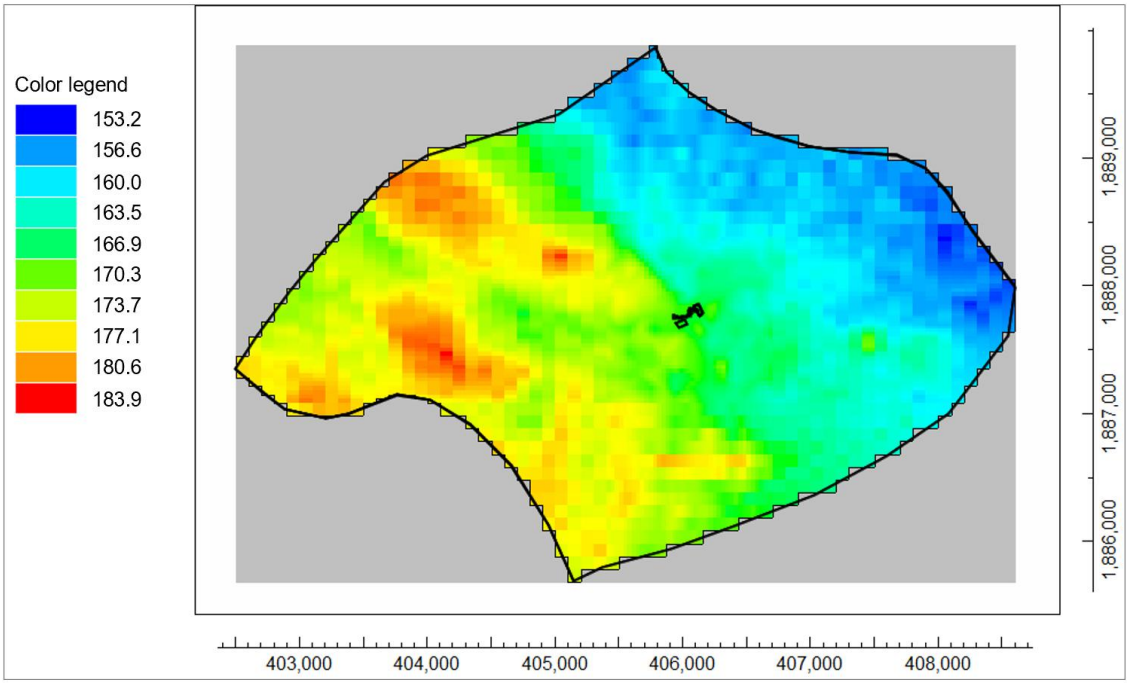


**Figure 16** Middle layer bottom elevation (m.a.s.l.).

### 3.1.4 Grid Design

In the simulation, the study area has been divided into 202 columns along the east-west direction and 151 rows in the north-south direction, resulting in a total of 63,320 grid cells across three layers of groundwater. Figures 17 illustrate the grid division for the study area. The specifics of the grid division are as follows:

1) East-West Direction: The area is segmented into 202 grid columns. The density of grid cells increases as one approaches the construction site of the MAR system.

- 40-meter grid cells: a total of 87 grid cells located in rows 1-55 and 171-202
- 30-meter grid cells: a total of 39 grid cells located in rows 56-75 and 152-170
- 20-meter grid cells: a total of 76 grid cells located in rows 76-151

2) North-South Direction: The area is subdivided into 151 rows. Similar to the east-west direction, the density of grid cells increases near the construction site of the MAR system.

- 40-meter grid cells: a total of 40 grid cells located in rows 1-19 and 131-151
- 30-meter grid cells: a total of 40 grid cells located in rows 20-39 and 111-130
- 20-meter grid cells: a total of 71 grid cells located in rows 40-110

This systematic organisation of grid cells is designed to facilitate accurate and efficient calculations throughout the simulation process.

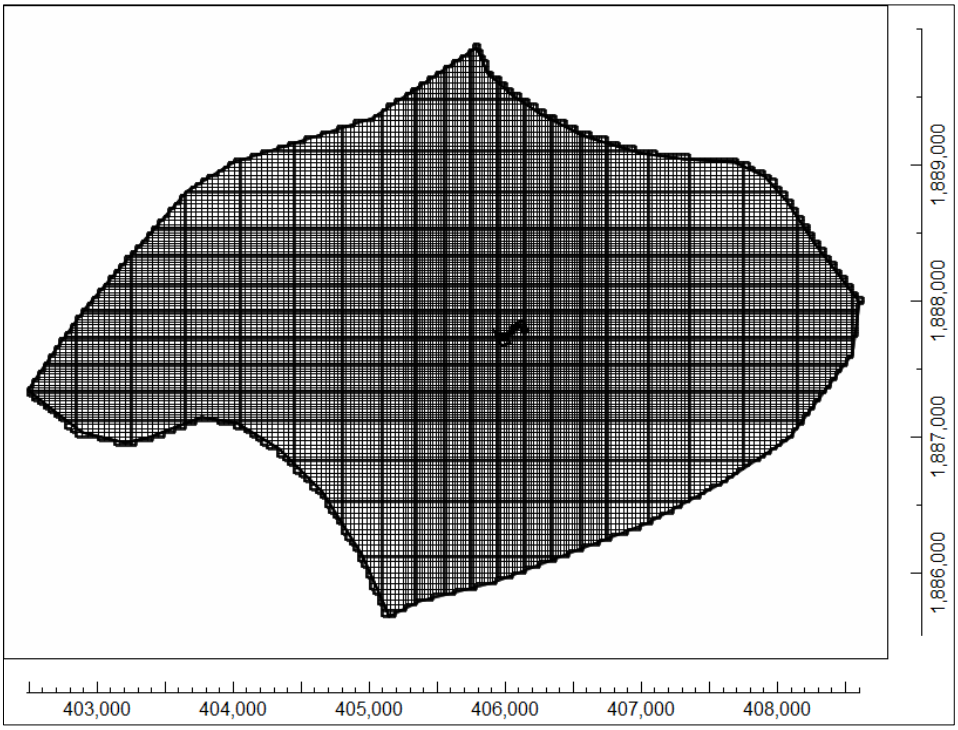


**Figure 17** Numerical grid of the study area.

### 3.1.5 Hydraulic properties

DGR conducted a slug test to assess the hydraulic conductivity of the middle layer in five observation wells (wells 1-6). The results are presented in Table 3.

**Table 3** The hydraulic conductivity (m/d) for the middle layer, measured from wells No.1-5, and for the lower layer, measured from well No.6.

| Well No. | Hydraulic conductivity (K) (m/d) |
|---|---|
| 1 | 0.504 |
| 2 | 0.835 |
| 3 | 0.504 |
| 4 | 0.596 |
| 5 | 0.278 |
| 6 | 0.382 |

According to Freeze (1984), as cited in Todd and Mays (2004), the hydraulic conductivity of clayey sand ranges from approximately 0.03 to 3 m/d. However, the hydraulic conductivity obtained from the assessment is lower than the values mentioned by Freeze (1984). This difference can occur because the hydraulic conductivity derived from slug tests is often underestimated, particularly in heterogeneous or unconsolidated sediments. Slug tests assess only a small portion of the aquifer, which may overlook higher conductivity zones that play a significant role in groundwater flow (Butler Jr, 2019). The initial horizontal hydraulic conductivity ($K_H$) and vertical hydraulic conductivity ($K_v$) of this study are given in Table 4. The $K_H$ of the upper unconfined aquifer is derived from the $K_H$ ranges of clayey sand, as referenced in Todd and Mays (2004). The $K_H$ for the middle layer is calculated by averaging the results from slug tests conducted on wells No. 1 to 5. Additionally, the $K_H$ for the lower layer is obtained from the slug test results of well No. 6. The $K_v$ determined for the simulation is equal to the hydraulic conductivity ($K_H$) divided by 10 (Winston, 2023).

**Table 4** Initial horizontal hydraulic conductivity of each layer.

| Layer | Geological Material | $K_H$ (m/d) | $K_v$ (m/d) |
|---|---|---|---|
| Upper Unconfined Aquifer | clayey sand (very fine to fine sand) | 0.5 | 0.05 |
| Middle Layer | clayey sand (fine to medium sand) | 0.543 | 0.0543 |
| Lower Layer | Shale | 0.382 | 0.0382 |

### 3.1.6 Recharge

Groundwater recharge refers to the process by which water from rainfall infiltrates through the topsoil and replenishes the groundwater layer. The rate at which groundwater is recharged depends on several factors, including average rainfall, evapotranspiration rates, and soil properties.

According to Freeze and Cherry (1979), Fetter (2018), and Scanlon (2006), clayey sand recharge tends to be low because fine sand has small pores, which can retain more water due to capillary forces. The approximate recharge percentages can be 10-20% of rainfall.

**1) Recharge rate of the study area**

The recharge rate was determined using the average rainfall and actual evapotranspiration rate data over the past twenty years, as shown in Table 5.

**Table 5** Monthly average rainfall and evapotranspiration rate over the past twenty years.

| Month | Rainfall (mm per month) | Evapotranspiration (mm per month) |
|---|---|---|
| **January** | 7.8 | 113.9 |
| **February** | 19.2 | 124.6 |
| **March** | 54.7 | 148.9 |
| **April** | 91.6 | 161.0 |
| **May** | 205.8 | 143.7 |
| **June** | 245.8 | 121.7 |
| **July** | 367.7 | 112.6 |
| **August** | 307.3 | 107.4 |
| **September** | 242.7 | 103.6 |
| **October** | 85.5 | 114.4 |
| **November** | 15.5 | 105.9 |
| **December** | 3.7 | 103.4 |
| **Total** | 1,647.3 | 1,461.1 |

The annual rainfall is 1,647.3 mm, while the total evapotranspiration rate is 1,461.1 mm per year. The recharge rate can be calculated as the difference between the average rainfall and the evapotranspiration rate. Thus,

$$\text{Potential Recharge} = \text{Annual Rainfall} - \text{Evapotranspiration rate} \quad (3.1)$$

$$\text{Recharge Rate} = 1{,}647.3 - 1{,}461.1 = 186.2 \text{ mm/year}$$

It can be defined as the percentage of rainfall as follows:

$$\text{Recharge Percentage} = \left(\frac{\text{Recharge Rate} \times 100}{\text{Annual Rainfall}}\right) \quad (3.2)$$

$$\text{Recharge Percentage} = \left(\frac{186.2 \times 100}{1647.3}\right) = 11.3033$$

The recharge rate for the study area is approximately 11.3% of the total rainfall. This percentage will serve as the recharge rate for the RCH package in the study area.

**2) Recharge of the MAR system**

The recharge rate was calculated based on the total rainfall, evapotranspiration rate, and changes in the water level of the MAR system, which includes the sediment basin, reservoir, and canal, as shown in Table 6-9.

**Table 6** Monthly rainfall and evapotranspiration rate in 2022.

| Month | Average Rainfall (mm per month) | Evapotranspiration (mm per month) |
|---|---|---|
| **January** | 1.6 | 107.5 |
| **February** | 38.8 | 107.5 |
| **March** | 62.8 | 132.9 |
| **April** | 25.8 | 139.9 |
| **May** | 250.2 | 106.6 |
| **June** | 122.2 | 122.6 |
| **July** | 223.7 | 120.4 |
| **August** | 174.1 | 109.4 |
| **September** | 232.9 | 103.0 |
| **October** | 049.9 | 118.4 |
| **November** | 022.9 | 107.7 |
| **December** | 0 | 110.4 |
| **Total** | 1,204.9 | 1,386.3 |

**Table 7** Monthly water level and water level change of the MAR system in 2022 (manual measurement by the Department of Groundwater Resources).

| Date | Water Level (m.a.s.l.) | | | Change in Water Level (m) | | |
|---|---|---|---|---|---|---|
| | Sediment Basin | Reservoir | Canal | Sediment Basin | Reservoir | Canal |
| **January** | 180.99 | 181.05 | 181.05 | 0.17 | -0.9 | -0.70 |
| **February** | 181.16 | 180.15 | 180.15 | -0.08 | -0.16 | -0.10 |
| **March** | 181.08 | 179.99 | 179.99 | -0.17 | -0.24 | -0.14 |
| **April** | 180.91 | 179.75 | 179.75 | 0.18 | 0.32 | 0.32 |
| **May** | 181.09 | 180.07 | 180.07 | 0.84 | 1.56 | 1.56 |
| **June** | 181.93 | 181.63 | 181.63 | 0.44 | 0.05 | 0.05 |
| **July** | 182.37 | 181.68 | 181.68 | -0.05 | 0.09 | 0.09 |
| **August** | 182.32 | 181.77 | 181.77 | -0.13 | 0.34 | 0.34 |
| **September** | 182.19 | 182.11 | 182.11 | -0.16 | -0.39 | -0.30 |
| **October** | 182.03 | 181.72 | 181.72 | -0.2 | -0.51 | -0.40 |
| **November** | 181.83 | 181.21 | 181.21 | -0.46 | -0.46 | -0.36 |
| **December** | 181.37 | 180.75 | 180.75 | -0.21 | -0.21 | -0.11 |

The recharge can be calculated from

$$\text{Recharge} = \text{Rainfall} - \text{Evapotranspiration} - \text{Storage Change} \quad (3.3)$$

Where Recharge is the groundwater recharge ($m^3$/month)

Rainfall is the volume of rainfall (average rainfall x the MAR area)

Evaporation is the volume of water evapotranspiration (ET x the MAR area)

Storage Change is the change in the volume of water in the MAR ($m^3$/month)

The area and depth of the MAR system is shown in the Table 8, and the monthly recharge of the MAR is explained in Table 9.

**Table 8** Area and depth of the MAR system.

| | Width (m) | Length (m) | Area ($m^2$) | Depth (m) | Bottom Elevation (m.a.s.l) |
|---|---|---|---|---|---|
| **Reservoir** | 40 | 80 | 3200 | 5 | 176 |
| **Sediment Basin** | 50 | 80 | 4000 | 5 | 178.3 |
| **Canal** | 18 | 200 | 3600 | 3 | 177.8 |

**Table 9** Evapotranspiration, rainfall, water storage volume changes, and groundwater recharge of the MAR system in m3/month in 2022.

| Date | Evapotranspiration ($m^3$/month) | | | Rainfall ($m^3$/month) | | | Storage Change ($\Delta S$) ($m^3$/month) | | | Groundwater Recharge ($m^3$/month) | | |
|---|---|---|---|---|---|---|---|---|---|---|---|---|
| | Sediment Basin | Reservoir | Canal | Sediment Basin | Reservoir | Canal | Sediment Basin | Reservoir | Canal | Sediment Basin | Reservoir | Canal |
| **January** | 430.0 | 344.0 | 387.0 | 14.2 | 11.3 | 12.7 | 680.0 | -2880.0 | -3240.0 | -1103.6 | 2541.1 | 2858.8 |
| **February** | 430.0 | 344.0 | 387.0 | 233.6 | 186.9 | 210.2 | -320.0 | -512.0 | -576.0 | 45.2 | 292.2 | 328.7 |
| **March** | 531.6 | 425.3 | 478.4 | 323.8 | 259.1 | 291.4 | -680.0 | -768.0 | -864.0 | 399.6 | 543.7 | 611.6 |
| **April** | 559.6 | 447.7 | 503.6 | 332.9 | 266.3 | 299.6 | 720.0 | 1024.0 | 1152.0 | -1176.4 | -1389.1 | -1562.8 |
| **May** | 426.4 | 341.1 | 383.8 | 1295.5 | 1036.4 | 1165.9 | 2360.0 | 4314.0 | 5616.0 | -1785.6 | -3854.5 | -5099.0 |
| **June** | 410.4 | 328.3 | 369.4 | 754.5 | 603.6 | 679.0 | 1264.0 | 160.0 | 180.0 | -1265.6 | -161.3 | -181.4 |
| **July** | 401.6 | 321.3 | 361.4 | 1116.1 | 892.9 | 1004.5 | -350.0 | 288.0 | 324.0 | 763.2 | 42.6 | 47.9 |
| **August** | 437.6 | 350.1 | 393.5 | 1240.8 | 992.7 | 1116.7 | -520.0 | 688.0 | 1224.0 | 778.8 | -481.0 | -991.1 |
| **September** | 412.0 | 329.6 | 370.8 | 1064.9 | 851.9 | 958.4 | -640.0 | -1248.0 | -1404.0 | 1159.6 | 1663.7 | 1871.6 |
| **October** | 473.6 | 378.9 | 426.2 | 164.4 | 131.5 | 147.9 | -800.0 | -1632.0 | -1836.0 | 526.0 | 1412.8 | 1589.4 |
| **November** | 430.8 | 344.6 | 387.7 | 100.9 | 80.8 | 90.9 | -1840.0 | -1472.0 | -1656.0 | 1500.8 | 1200.6 | 1350.7 |
| **December** | 401.6 | 321.3 | 361.4 | 0 | 0 | 0 | -840.0 | -672.0 | -756.0 | 398.4 | 318.7 | 358.6 |
| **Total** | 5345.2 | 4276.2 | 4810.2 | 6641.6 | 5313.4 | 5977.2 | -966.0 | -2710.0 | -1836.0 | 240.4 | 2129.52 | 1182.46 |

According to Table 9, the total rainfall recorded in 2022 was 17,932.43 cubic meters ($m^3$), while the total recharge amounted to 3,552.38 $m^3$. This means that the recharge represents approximately 19.81% of the total rainfall. For the purpose of this study, this percentage will be used as the recharge rate for the RCH package in the MAR system.

**3) Future precipitation**

The rainfall in the next ten years, from 2025 to 2034, was estimated using the trend projection (Appendix A) based on the least squares technique. This method is a recognised approach for analysing and forecasting time series data by fitting a mathematical function, usually a straight line, to historical data while minimising the sum of squared differences between observed and estimated values (Wolberg, 2006). The resulting linear trend equation helps identify long-term patterns and project future rainfall. The least squares equation is expressed as:

$$y_t = a + bt \tag{3.4}$$

Where $y_t$ is predicted value at time t

$a$ is the intercept (value of y when t=0)

$b$ is the slope of the trend line

$t$ is time

The future rainfall was estimated on a monthly basis for the period from 2025 to 2034, as shown in Table 10.

**Table 10** Monthly estimated rainfall from 2025 to 2034 (mm).

| Least squares equation | y=-0.0923x+ 8.7237 | y=0.3626x+15.353 | y =-0.1889x + 56.629 | y =-4.149x + 135.14 | y =-4.6735x + 254.87 | y =-0.9091x + 255.37 | y =-1.6828x + 385.33 | y =-4.4935x + 354.44 | y =2.4907x + 216.59 | y =-3.3732x + 120.9 | y =-2.3186x + 38.187 | y =-0.2281x + 6.1694 |
|---|---|---|---|---|---|---|---|---|---|---|---|---|
| **Year** | **Jan** | **Feb** | **Mar** | **Apr** | **May** | **Jun** | **Jul** | **Aug** | **Sep** | **Oct** | **Nov** | **Dec** |
| 2025 | 6.8 | 23.0 | 52.7 | 37.0 | 156.7 | 236.3 | 350.0 | 260.1 | 268.9 | 50.1 | 0.0 | 0.0 |
| 2026 | 6.7 | 23.3 | 52.5 | 32.3 | 152.1 | 235.4 | 348.3 | 255.6 | 271.4 | 46.7 | 0.0 | 0.0 |
| 2027 | 6.6 | 23.7 | 52.3 | 27.7 | 147.4 | 234.5 | 346.6 | 251.1 | 273.9 | 43.3 | 0.0 | 0.0 |
| 2028 | 6.5 | 24.1 | 52.1 | 23.0 | 142.7 | 233.6 | 344.9 | 246.6 | 276.4 | 39.9 | 0.0 | 0.0 |
| 2029 | 6.4 | 24.4 | 51.9 | 18.3 | 138.0 | 232.6 | 343.3 | 242.1 | 278.9 | 36.6 | 0.0 | 0.0 |
| 2030 | 6.3 | 24.8 | 51.7 | 13.6 | 133.4 | 231.7 | 341.6 | 237.6 | 281.4 | 33.2 | 0.0 | 0.0 |
| 2031 | 6.2 | 25.1 | 51.5 | 9.0 | 128.7 | 230.8 | 339.9 | 233.1 | 283.8 | 29.8 | 0.0 | 0.0 |
| 2032 | 6.1 | 25.5 | 51.3 | 4.3 | 124.0 | 229.9 | 338.2 | 228.6 | 286.3 | 26.5 | 0.0 | 0.0 |
| 2033 | 6.1 | 25.9 | 51.2 | -0.4 | 119.3 | 229.0 | 336.5 | 224.1 | 288.8 | 23.1 | 0.0 | 0.0 |
| 2034 | 6.0 | 26.2 | 51.0 | -5.1 | 114.7 | 228.1 | 334.9 | 219.6 | 291.3 | 19.7 | 0.0 | 0.0 |

**4) Recharge rate**

According to section 3.6.1, the recharge rate for the study area is approximately 11.33% of the total rainfall, while the recharge rate of the MAR system is about 19.81% of the total rainfall. The recharge rates of the study area and the MAR are summarised in Tables 11 and 12, respectively.

### 3.1.7 Evapotranspiration

Evapotranspiration rates are influenced by factors such as solar radiation, temperature, relative humidity, wind speed, and hours of sunshine. The least squares equation from the trendline (Appendix B) was applied to calculate the monthly evapotranspiration rate for the years 2025-2034, as shown in Table 13.

### 3.1.8 Water use

The water used in the study area is sourced from the groundwater wells, which serve as the primary water source for the population and draw water directly from a shallow aquifer that has been impacted by the construction of the MAR system. The wells are situated in the direction where water from the MAR system flows toward them.

**Table 11** Monthly recharge rates of the study area from 2020 to 2034 (mm).

| Year | Jan | Feb | Mar | Apr | May | Jun | Jul | Aug | Sep | Oct | Nov | Dec |
|---|---|---|---|---|---|---|---|---|---|---|---|---|
| 2020 | 2.4 | 0.0 | 13.6 | 3.3 | 22.4 | 16.6 | 25.9 | 30.4 | 14.4 | 16.4 | 0.1 | 0.0 |
| 2021 | 0.0 | 2.4 | 9.6 | 17.4 | 10.3 | 31.3 | 32.2 | 17.9 | 20.7 | 19.9 | 0.0 | 0.0 |
| 2022 | 0.2 | 4.4 | 7.1 | 2.9 | 28.3 | 13.8 | 25.3 | 19.7 | 26.4 | 5.7 | 2.6 | 0.0 |
| 2023 | 2.1 | 0.8 | 0.2 | 4.1 | 12.4 | 44.2 | 47.9 | 37.0 | 65.0 | 9.4 | 0.0 | 0.0 |
| 2024 | 0.0 | 0.4 | 1.6 | 3.3 | 20.9 | 16.4 | 30.4 | 50.1 | 37.2 | 1.2 | 0.0 | 0.0 |
| 2025 | 0.8 | 2.6 | 6.0 | 4.2 | 17.8 | 26.8 | 39.7 | 29.5 | 30.5 | 5.7 | 0.0 | 0.0 |
| 2026 | 0.8 | 2.6 | 5.9 | 3.7 | 17.2 | 26.7 | 39.5 | 29.0 | 30.7 | 5.3 | 0.0 | 0.0 |
| 2027 | 0.7 | 2.7 | 5.9 | 3.1 | 16.7 | 26.6 | 39.3 | 28.4 | 31.0 | 4.9 | 0.0 | 0.0 |
| 2028 | 0.7 | 2.7 | 5.9 | 2.6 | 16.2 | 26.5 | 39.1 | 27.9 | 31.3 | 4.5 | 0.0 | 0.0 |
| 2029 | 0.7 | 2.8 | 5.9 | 2.1 | 15.6 | 26.4 | 38.9 | 27.4 | 31.6 | 4.1 | 0.0 | 0.0 |
| 2030 | 0.7 | 2.8 | 5.9 | 1.5 | 15.1 | 26.3 | 38.7 | 26.9 | 31.9 | 3.8 | 0.0 | 0.0 |
| 2031 | 0.7 | 2.8 | 5.8 | 1.0 | 14.6 | 26.2 | 38.5 | 26.4 | 32.2 | 3.4 | 0.0 | 0.0 |
| 2032 | 0.7 | 2.9 | 5.8 | 0.5 | 14.1 | 26.0 | 38.3 | 25.9 | 32.4 | 3.0 | 0.0 | 0.0 |
| 2033 | 0.7 | 2.9 | 5.8 | 0.0 | 13.5 | 25.9 | 38.1 | 25.4 | 32.7 | 2.6 | 0.0 | 0.0 |
| 2034 | 0.7 | 3.0 | 5.8 | -0.6 | 13.0 | 25.8 | 37.9 | 24.9 | 33.0 | 2.2 | 0.0 | 0.0 |

**Table 12** Monthly recharge rates of the MAR system from 2022 to 2034 (mm).

| Year | Jan | Feb | Mar | Apr | May | Jun | Jul | Aug | Sep | Oct | Nov | Dec |
|---|---|---|---|---|---|---|---|---|---|---|---|---|
| 2022 | 0.3 | 7.7 | 12.4 | 5.1 | 49.6 | 24.2 | 44.3 | 34.5 | 46.1 | 9.9 | 4.5 | 0.0 |
| 2023 | 3.7 | 1.3 | 0.3 | 7.1 | 21.7 | 77.3 | 83.8 | 64.6 | 113.6 | 16.5 | 0.0 | 0.0 |
| 2024 | 0.0 | 0.6 | 2.8 | 5.7 | 36.5 | 28.7 | 53.1 | 87.5 | 65.0 | 2.0 | 0.0 | 0.0 |
| 2025 | 1.3 | 4.6 | 10.4 | 7.3 | 31.0 | 46.8 | 69.3 | 51.5 | 53.3 | 9.9 | 0.0 | 0.0 |
| 2026 | 1.3 | 4.6 | 10.4 | 6.4 | 30.1 | 46.6 | 69.0 | 50.6 | 53.8 | 9.2 | 0.0 | 0.0 |
| 2027 | 1.3 | 4.7 | 10.4 | 5.5 | 29.2 | 46.4 | 68.7 | 49.7 | 54.3 | 8.6 | 0.0 | 0.0 |
| 2028 | 1.3 | 4.8 | 10.3 | 4.6 | 28.3 | 46.3 | 68.3 | 48.9 | 54.7 | 7.9 | 0.0 | 0.0 |
| 2029 | 1.3 | 4.8 | 10.3 | 3.6 | 27.3 | 46.1 | 68.0 | 48.0 | 55.2 | 7.2 | 0.0 | 0.0 |
| 2030 | 1.3 | 4.9 | 10.2 | 2.7 | 26.4 | 45.9 | 67.7 | 47.1 | 55.7 | 6.6 | 0.0 | 0.0 |
| 2031 | 1.2 | 5.0 | 10.2 | 1.8 | 25.5 | 45.7 | 67.3 | 46.2 | 56.2 | 5.9 | 0.0 | 0.0 |
| 2032 | 1.2 | 5.1 | 10.2 | 0.8 | 24.6 | 45.5 | 67.0 | 45.3 | 56.7 | 5.2 | 0.0 | 0.0 |
| 2033 | 1.2 | 5.1 | 10.1 | -0.1 | 23.6 | 45.4 | 66.7 | 44.4 | 57.2 | 4.6 | 0.0 | 0.0 |
| 2034 | 1.2 | 5.2 | 10.1 | -1.0 | 22.7 | 45.2 | 66.3 | 43.5 | 57.7 | 3.9 | 0.0 | 0.0 |

**Table 13** Monthly estimated evapotranspiration from 2025 to 2034 (mm).

| Least squares equation | y =-0.6768x + 1477.41 | y =-0.2429x + 613.99 | y =-1.0732x + 2311.8 | y =0.5979x - 1043.5 | y =0.5148x - 893.38 | y =0.2728x - 427.8 | y =0.141x - 171.93 | y =0.2457x - 389.54 | y =-0.0712x +250.54 | y =-0.1298x + 381.98 | y =-0.402x + 924.39 | y =-0.2796x + 672.16 |
|---|---|---|---|---|---|---|---|---|---|---|---|---|
| **Year** | **Jan** | **Feb** | **Mar** | **Apr** | **May** | **Jun** | **Jul** | **Aug** | **Sep** | **Oct** | **Nov** | **Dec** |
| 2025 | 106.9 | 122.1 | 138.6 | 167.3 | 149.1 | 124.6 | 113.6 | 108.0 | 106.4 | 119.1 | 110.3 | 106.0 |
| 2026 | 106.2 | 121.9 | 137.5 | 167.9 | 149.6 | 124.9 | 113.7 | 108.3 | 106.3 | 119.0 | 109.9 | 105.7 |
| 2027 | 105.5 | 121.6 | 136.4 | 168.4 | 150.1 | 125.2 | 113.9 | 108.5 | 106.2 | 118.9 | 109.5 | 105.4 |
| 2028 | 104.9 | 121.4 | 135.4 | 169.0 | 150.6 | 125.4 | 114.0 | 108.7 | 106.2 | 118.8 | 109.1 | 105.1 |
| 2029 | 104.2 | 121.2 | 134.3 | 169.6 | 151.2 | 125.7 | 114.2 | 109.0 | 106.1 | 118.6 | 108.7 | 104.9 |
| 2030 | 103.5 | 120.9 | 133.2 | 170.2 | 151.7 | 126.0 | 114.3 | 109.2 | 106.0 | 118.5 | 108.3 | 104.6 |
| 2031 | 102.8 | 120.7 | 132.1 | 170.8 | 152.2 | 126.3 | 114.4 | 109.5 | 105.9 | 118.4 | 107.9 | 104.3 |
| 2032 | 102.1 | 120.4 | 131.1 | 171.4 | 152.7 | 126.5 | 114.6 | 109.7 | 105.9 | 118.2 | 107.5 | 104.0 |
| 2033 | 101.5 | 120.2 | 130.0 | 172.0 | 153.2 | 126.8 | 114.7 | 110.0 | 105.8 | 118.1 | 107.1 | 103.7 |
| 2034 | 100.8 | 119.9 | 128.9 | 172.6 | 153.7 | 127.1 | 114.9 | 110.2 | 105.7 | 118.0 | 106.7 | 103.5 |

### 3.1.9 Hydraulic head observation

Groundwater level data plays a crucial role in verifying the model results. Every season, groundwater level readings are collected from 5 observation wells surrounding the construction area of the MAR, as well as from 13 groundwater wells distributed throughout the study area by the DRG (Figure 18). This data is used to monitor water level changes and compare with groundwater levels or groundwater pressure obtained from the model. Such comparisons are essential for enhancing the reliability of the model. The water levels of the observation wells and groundwater wells are illustrated in Table 14.

**Table 14** Measurements of water levels of the observation wells and groundwater wells.

| Well Number | OBS value (m.a.s.l.) | | Pumping rate ($m^3$/day) |
|---|---|---|---|
| | June 2021 (Without MAR) | June 2022 (With MAR) | |
| 6410D001 | 182.93 | 184.23 | 0 |
| 6410D002 | 183.85 | 183.89 | 0 |
| 6410D003 | 183.20 | 183.69 | 0 |
| 6410D004 | 183.28 | 183.65 | 0 |
| 6410D005 | 182.60 | 183.56 | 0 |
| Well7 | 182.87 | 183.90 | 0 |
| Well9 | 182.53 | 183.60 | 0 |
| Well10 | 180.24 | 180.68 | 0 |
| Well11 | 180.59 | 180.71 | 30 |
| Well12 | 176.31 | 176.03 | 35 |
| Well13 | 177.12 | 177.26 | 0 |
| Well14 | 176.94 | 177.11 | 0 |
| Well15 | 175.81 | 175.69 | 0 |
| Well16 | 177.30 | 177.41 | 0 |
| Well17 | 175.06 | 175.39 | 0 |
| Well31 | 184.63 | 184.42 | 0 |
| Well37 | 188.83 | 188.02 | 15 |
| Well56 | 181.10 | 181.46 | 0 |

Figure removed due to copyright restriction.

**Figure 18** Location of the observation wells and groundwater wells that are used to monitor the water level in the study area.

### 3.1.10 Summary of model setup and model package

Table 15 provides a summary of the important details regarding the setup of the MODFLOW model.

**Table 15** Summary of the model setup and packages used to set the features.

| Object | Package | Feature | Value | Unit |
|---|---|---|---|---|
| No-flow boundary | The package was not used but set as an Inactive cell in the Data Set (Hughes et al., 2017) | - | - | - |
| Constant head | Time-Variant Specified-Head Package (CHD) (Harbaugh, 2005) | Head | 168 and 190 | m.a.s.l. |
| River (Reservoir before constructing the MAR) | River Package (RIV) (Harbaugh, 2005) | River Stage | Water levels change with the seasons. | m.a.s.l. |
| | | River Bottom | Model_Top - 3 | m.a.s.l. |
| | | Conductance | Kz[1]/1.5 | 1/d |
| | | Hydraulic Conductivity | $10^{-2}$ to 1[2] | m/d |
| River (Reservoir after constructing the MAR) | River Package (RIV) (Harbaugh, 2005) | River Stage | Water levels change with the seasons. | m.a.s.l. |
| | | River Bottom | Model_Top - 5 | m.a.s.l. |
| | | Conductance | Kz[1]/0.2 | 1/d |
| | | Hydraulic Conductivity | $10^{-1}$ to 1[2] | m/d |
| River (Sediment basin before constructing the MAR) | River Package (RIV) (Harbaugh, 2005) | River Stage | Water levels change with the seasons. | m.a.s.l. |
| | | River Bottom | Model_Top – 2.5 | m.a.s.l. |
| | | Conductance | Kz[1]/1.5 | 1/d |
| | | Hydraulic Conductivity | $10^{-2}$ to 1[2] | m/d |

**Table 15** Summary of the model setup and Package is used to set the features (continue).

| Object | Package | Feature | Value | Unit |
|---|---|---|---|---|
| River (Sediment basin after constructing the MAR) | River Package (RIV) (Harbaugh, 2005) | River Stage | Water levels change with the seasons. | m.a.s.l. |
| | | River Bottom | Model_Top - 5 | m.a.s.l. |
| | | Conductance | Kz[1]/0.5 | 1/d |
| | | Hydraulic Conductivity | $10^{-1}$ to 1[2] | m/d |
| River (Canal before constructing the MAR) | River Package (RIV) (Harbaugh, 2005) | River Stage | Water levels change with the seasons. | m.a.s.l. |
| | | River Bottom | Model_Top – 2.45 | m.a.s.l. |
| | | Conductance | Kz[1]/1 | 1/d |
| | | Hydraulic Conductivity | $10^{-2}$ to 1[2] | m/d |
| River (Canal after constructing the MAR) | River Package (RIV) (Harbaugh, 2005) | River Stage | Water levels change with the seasons. | m.a.s.l. |
| | | River Bottom | Model_Top - 4 | m.a.s.l. |
| | | Conductance | Kz[1]/0.3 | 1/d |
| | | Hydraulic Conductivity | $10^{-1}$ to 1[2] | m/d |
| Recharge (Study Area) | Recharge Package (RCH) (Harbaugh, 2005) | Recharge rate | Shown in Table 11 | m/d |
| Recharge (MAR system) | Recharge Package (RCH) (Harbaugh, 2005) | Recharge rate | Shown in Table 12 | m/d |
| Evapotranspiration | Evapotranspiration Segments package (ETS) (Banta, 2000) | ET Rate | Shown in Tables 2 and 13 | m/d |
| | | ET surface | Model_Top | |
| | | ET depth | 2 | m |

**Table 15** Summary of the model setup and Package is used to set the features (continue).

| Object | Package | Feature | Value | Unit |
|---|---|---|---|---|
| Pumping Wells | Well Package (WEL) (Harbaugh, 2005) | Well No. | Shown in Table 14 | |
| | | Pumping Rate | Shown in Table 14 | $m^3/d$ |
| Observation Wells | Observation Utility Package (OBS) (Winston, 2019) | OBS Name | Shown in Table 14 | - |
| | | OBS Series Type | General | - |
| | | OBS Type | Head | - |
| | | OBS Value (OBSVAL) | Shown in Table 14 | m.a.s.l. |
| | | OBS Weight (WEIGHT) | 1 | - |
| Aquifer | The package was not used, but needs to define the hydraulic conductivity ($K_H$) for each layer | Upper Unconfined Aquifer (very fine to fine sand) | 0.1 to 10[2][3] | m/d |
| | | Middle Layer (fine to medium sand) | 1 to 100[2][3] | m/d |
| | | Lower Layer (shale) | $10^{-6}$ to 1[2][3] | m/d |

NOTE: [1] Kz is equal to hydraulic conductivity (Kx)/10 (Winston, 2023)

[2] Freeze and Cherry, 1979, cited in Todd and Mays 2004.

[3] Fetter, 2018

### 3.1.11 Model calibration

The model was calibrated manually by adjusting its parameters until the calculated groundwater level aligned with the field measurements, ensuring it fell within an acceptable range of the Root Mean Square Residual (RMSR). The RMSR difference between the calculated and measured values indicates the model's appropriateness and reliability. However, there isn't a universally accepted RMSR threshold. Generally, the residual difference between simulated results and real field conditions should be under 10 percent of the variability observed in field data throughout the entire model domain (Department of Environment, Great Lakes, and Energy, 2025). This study considers an RMSR value of less than 1.3 m acceptable, taking into account other factors, such as whether the direction of groundwater flow matches the real environment. Additionally, it evaluates whether the groundwater map displays a distribution of groundwater pressure that is similar to the model's results.

**1) First simulation**

According to Table 4, values of 0.5, 0.543, and 0.382 m/day were assigned as the hydraulic conductivity ($K_H$) for the upper unconfined aquifer, middle layer, and lower layer, respectively.

The water levels in the observation and pumping wells in June 2021 were used as calibration data. The simulation results, without calibration, indicate an RMSR of 4.99 m, which corresponds to a very high simulated head of 18 wells, as shown in Figure 19 and Table 16.

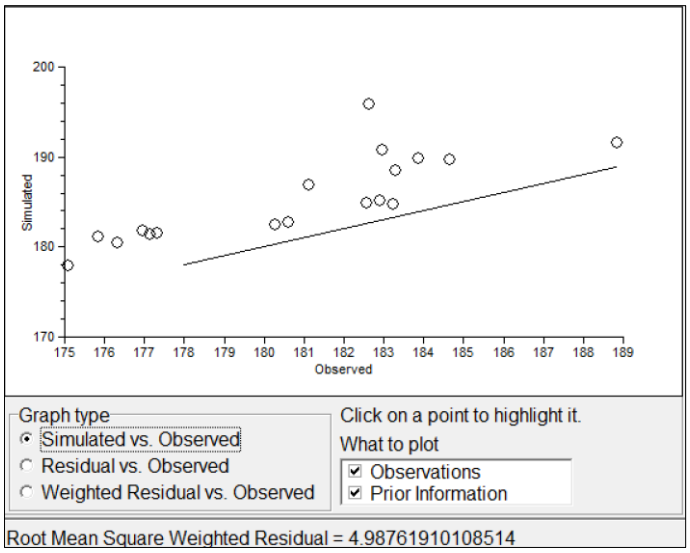


**Figure 19** Simulated head vs observation head and RMSR of the first simulation.

**Table 16** Simulated head and residual of the first simulation.

| Well Number | Measured Head (m.a.s.l.) | Simulated Head (m.a.s.l.) | Residual |
|---|---|---|---|
| 6410D001 | 182.93 | 190.93 | -8.00 |
| 6410D002 | 183.85 | 189.90 | -6.05 |
| 6410D003 | 183.20 | 184.82 | -1.62 |
| 6410D004 | 183.28 | 188.62 | -5.34 |
| 6410D005 | 182.60 | 195.97 | -13.37 |
| Well7 | 182.87 | 184.99 | -2.46 |
| Well9 | 182.53 | 185.31 | -2.44 |
| Well10 | 180.24 | 182.59 | -2.35 |
| Well11 | 180.59 | 182.85 | -2.26 |
| Well12 | 176.31 | 180.54 | -4.23 |
| Well13 | 177.12 | 181.47 | -4.35 |
| Well14 | 176.94 | 181.87 | -4.93 |
| Well15 | 175.81 | 181.22 | -5.41 |
| Well16 | 177.30 | 181.70 | -4.40 |
| Well17 | 175.06 | 177.99 | -2.93 |
| Well31 | 184.63 | 189.81 | -5.18 |
| Well37 | 188.83 | 191.64 | -2.81 |
| Well56 | 181.10 | 187.05 | -5.95 |

**2) Adjusted parameters**

The hydraulic conductivity ($K_H$) of the three layers was adjusted to achieve the minimum RMSR. The adjustment process began with the $K_H$ of the middle layer, which is the primary layer affected by managed aquifer recharge (MAR).

Initially, the $K_H$ was increased by 200% until the minimum RMSR was reached. After that, the adjusted $K_H$ was adjusted by making smaller adjustments of 10% to minimise the RMSR further. Similarly, the $K_H$ of the upper unconfined aquifer and the lower layer was increased by 10% until the model achieved the minimum RMSR. The adjusted $K_H$ of each layer are shown in Figures 20-22.

The most significant increase in hydraulic conductivity was observed in the middle layer, which increased by a factor of 51. This was followed by the upper unconfined aquifer and the lower layer, which increased by 3 and 2.3 times, respectively (Table 18).

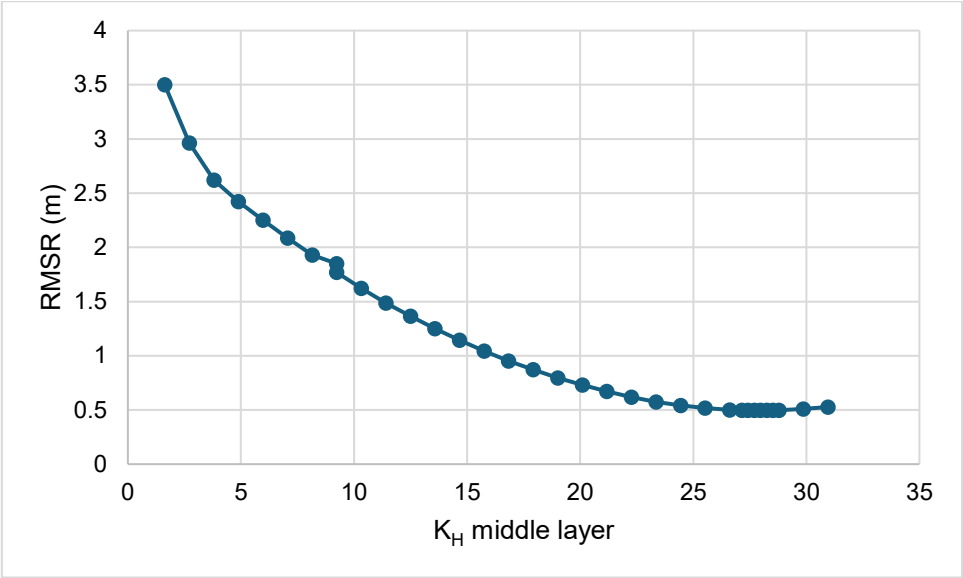


**Figure 20** Graph shows the RMSR when adjusting the $K_H$ of the middle layer.

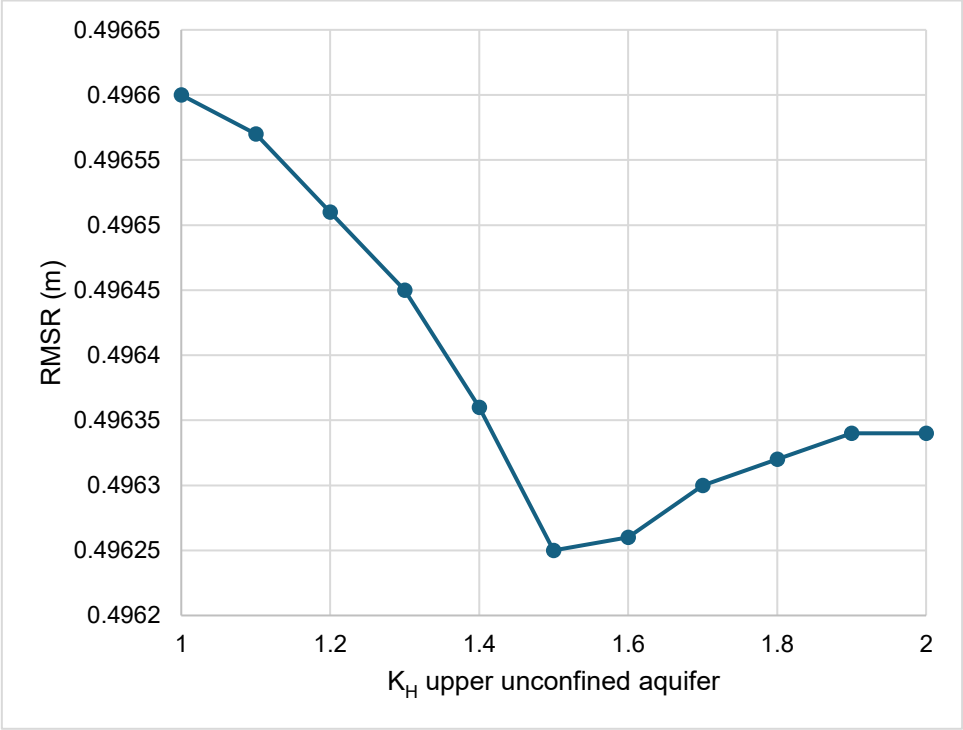


**Figure 21** Graph shows the RMSR when adjusting the $K_H$ of the upper unconfined aquifer.

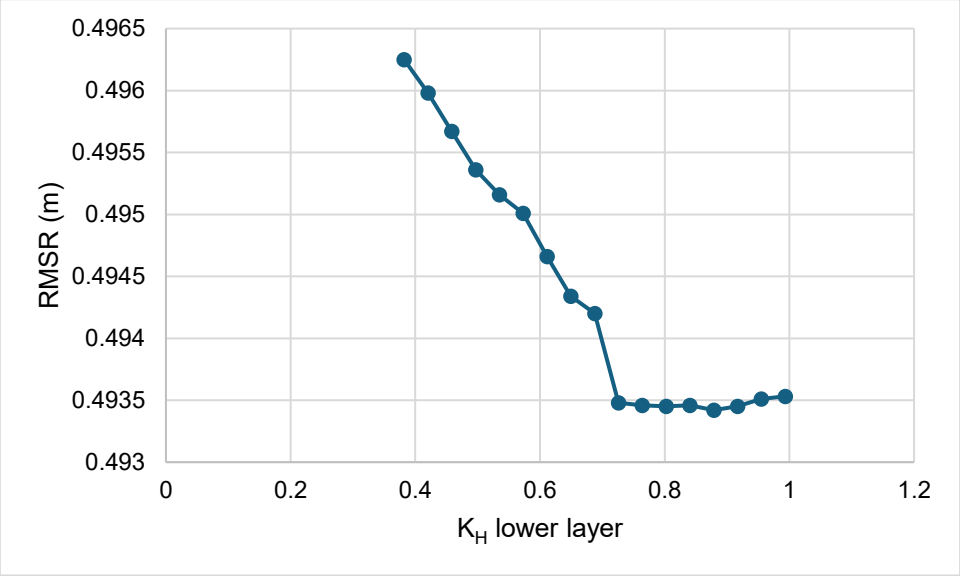


**Figure 22** Graph shows the RMSR when adjusting the $K_H$ of the lower layer.

**Table 17** Hydraulic conductivity of the three layers in the first simulation and the adjusted simulation.

| Layer | 1st Simulation | | Factor | Adjusted Simulation | |
|---|---|---|---|---|---|
| | $K_H$ (m/day) | $K_V$ (m/day) | | $K_H$ (m/day) | $K_V$ (m/day) |
| Upper Unconfined Aquifer | 0.5 | 0.05 | X3.00 | 1.5 | 0.15 |
| Middle Layer | 0.543 | 0.0543 | X51.00 | 27.69 | 2.769 |
| Lower Layer | 0.382 | 0.0382 | X2.30 | 0.88 | 0.088 |

After adjusting the hydraulic conductivity values, the simulated vs. observed graph shows a good match between the simulated and observed heads. As a result, the RMSR is 0.49 m (Figure 23). According to Butler Jr. (2019), slug tests evaluate only a limited section of the aquifer. This can result in estimated hydraulic conductivity values that are lower than the actual values, as these tests might miss higher conductivity zones that play a significant role in groundwater flow. Consequently, it can be assumed that the hydraulic conductivity values adjusted from the model are accurate and realistic.

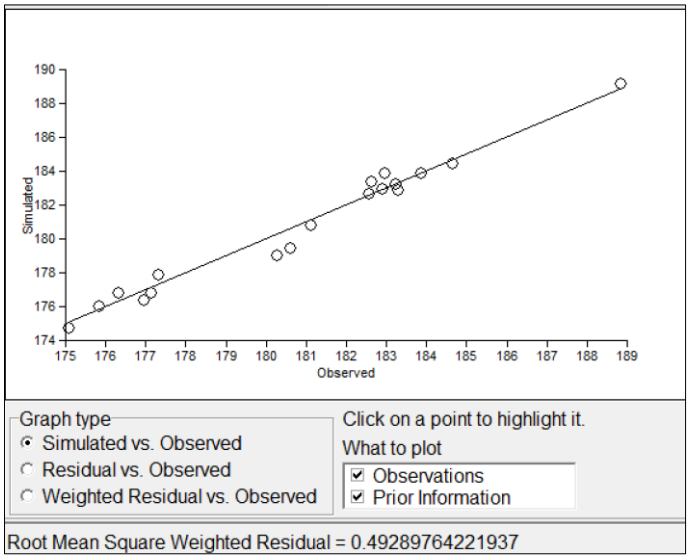


**Figure 23** Simulated head vs observation head and RMSR before constructing the MAR system, calibration using the water level in June 2021.

Following the establishment of the MAR system, the water levels from the observation and pumping wells, as recorded from June 2022, were used as calibration data. The graph comparing simulated and observed data displays a strong correlation between the simulated and observed heads. Consequently, the RMSR value is recorded at 0.53 m (Figure 24).

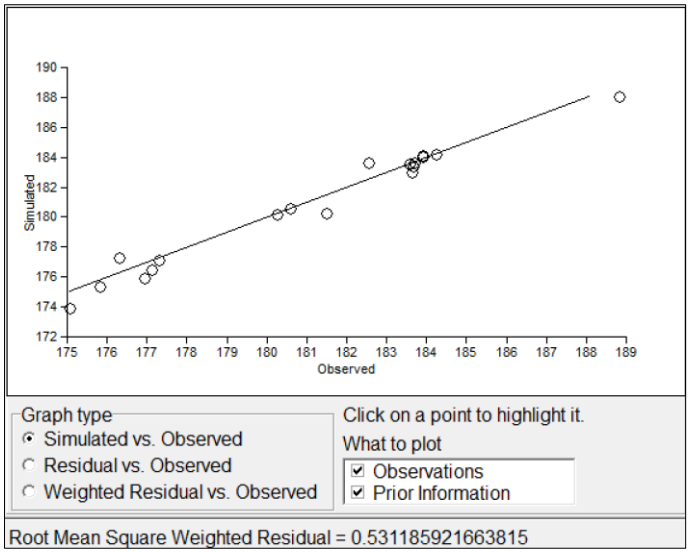


**Figure 24** Simulated head vs observation head and RMSR after constructing the MAR system, calibration using the water level in June 2022.

### 3) Sensitivity analysis

According to Table 18, the most sensitive parameter is the hydraulic conductivity of the middle layer, which is the primary aquifer for the recharge from the MAR system. This is followed by the hydraulic conductivity of the upper unconfined aquifer and then the lower layer, respectively.

## 3.2 Model Result

The water table model indicates that areas far from the MAR system will remain unchanged over the next 10 years (Figure 25). Additionally, it has proven difficult to detect differences in water levels at the MAR system when comparing periods with and without the system. As a result, a new boundary was established based on the model's water table results to narrow the study area and focus on the region surrounding the MAR system, as illustrated in Figure 26.

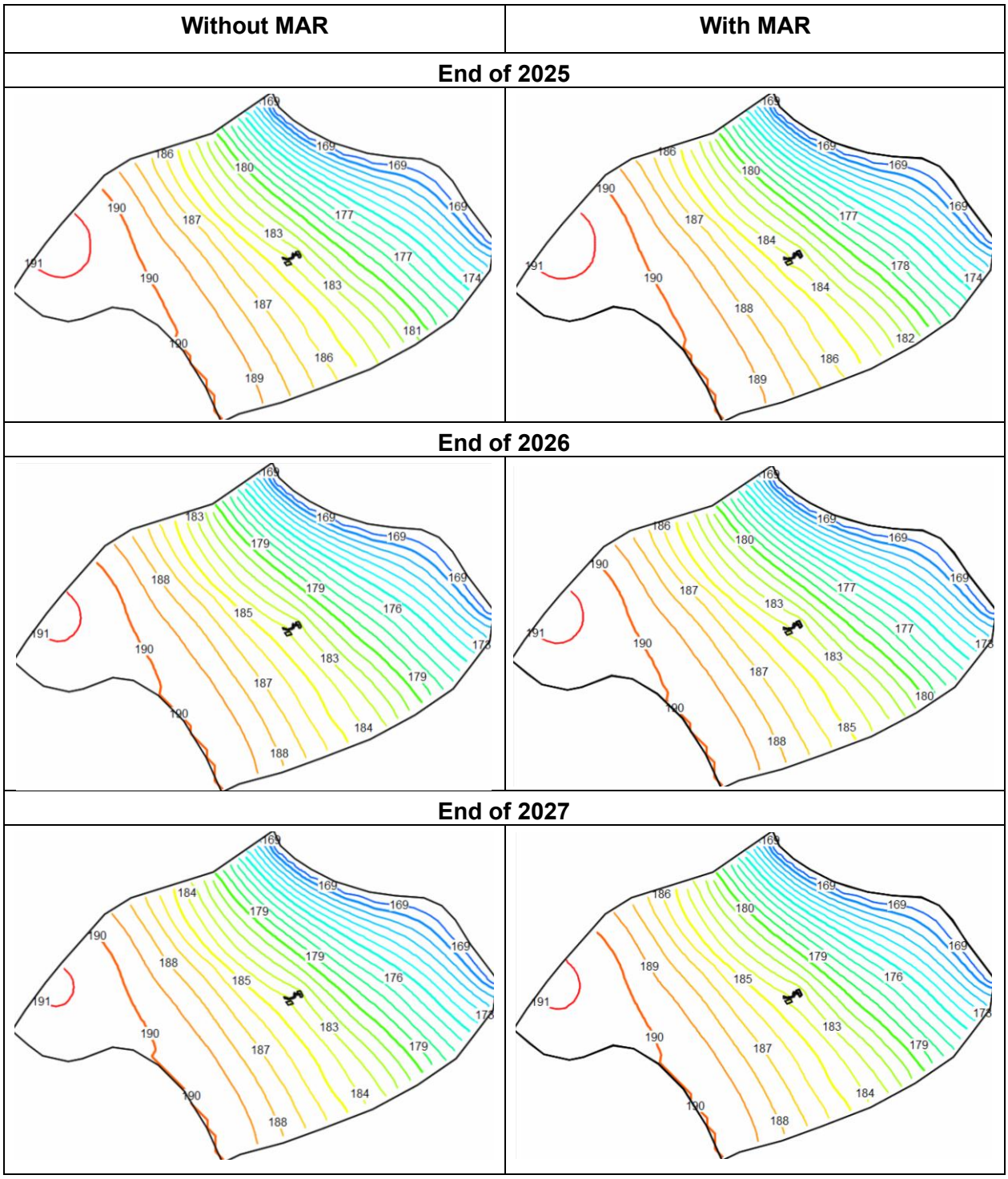


**Figure 25** Water level from the model's result in the wet season.

| Without MAR | With MAR |
|---|---|
| **End of 2028** | |
| 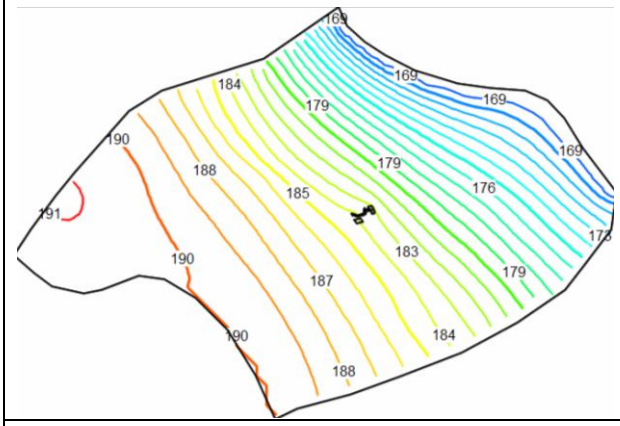 | 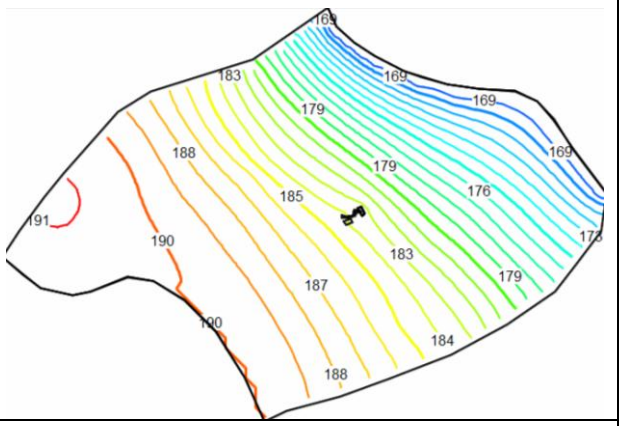 |
| **End of 2029** | |
| 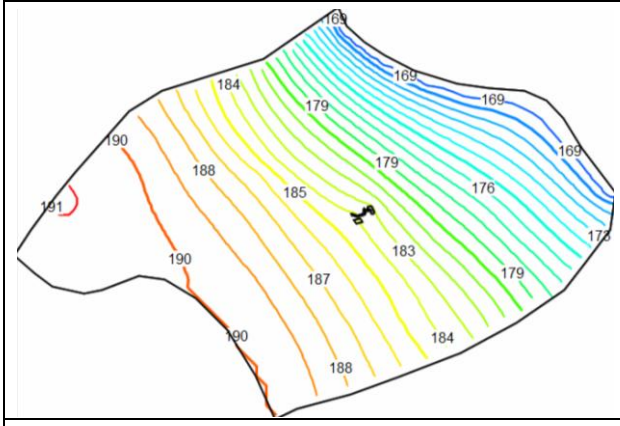 | 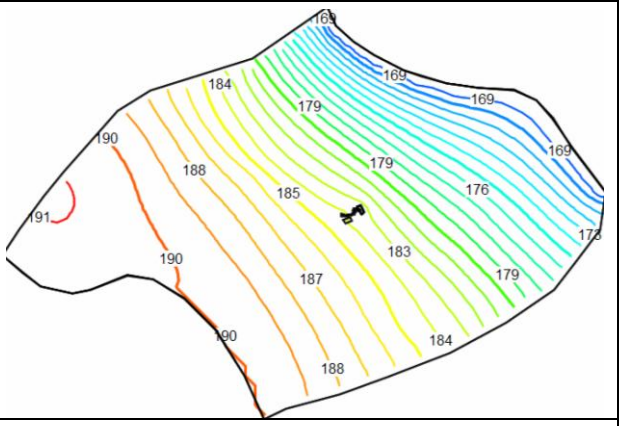 |
| **End of 2031** | |
| 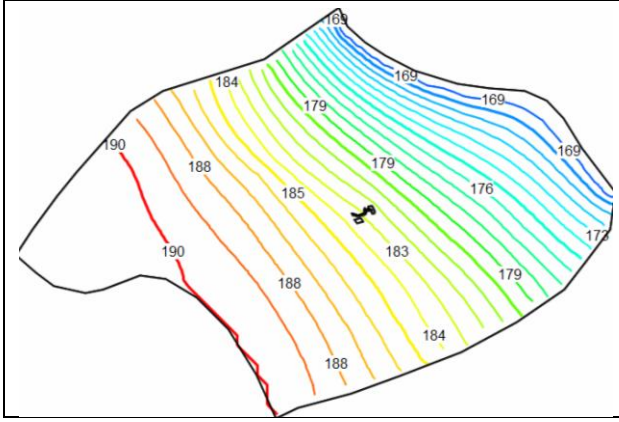 | 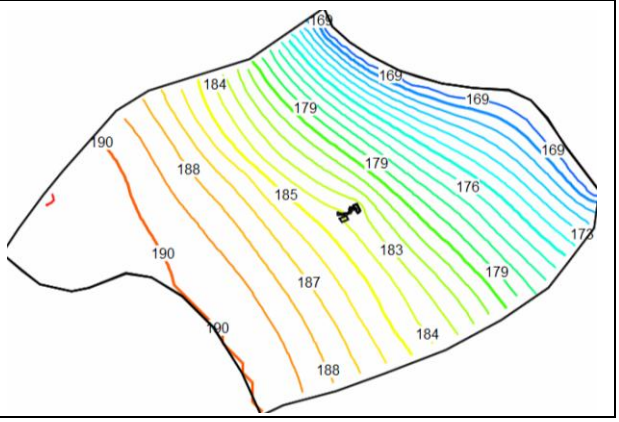 |

**Figure 25** Water level from the model result in the wet season (continue).

| Without MAR | With MAR |
|---|---|
| End of 2034 | |

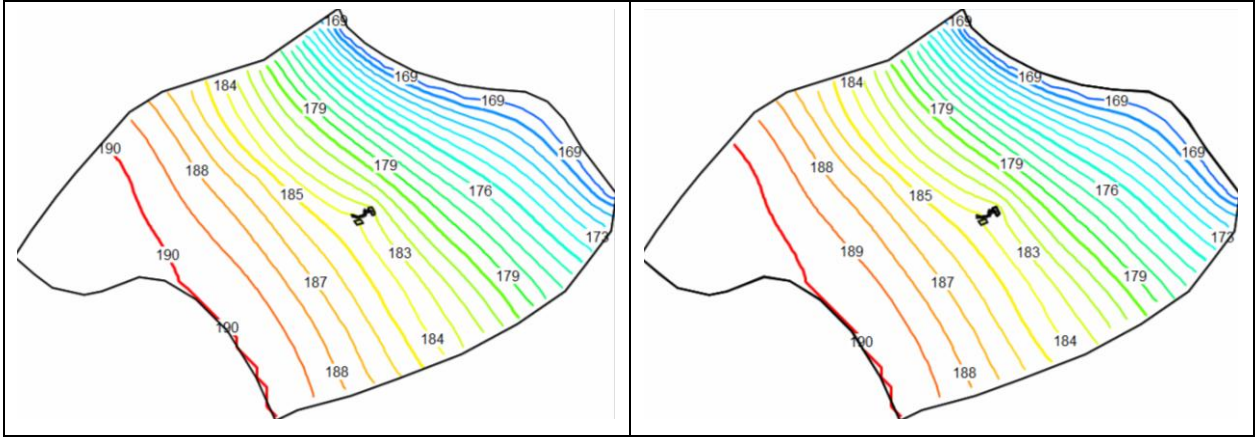


**Figure 25** Water level from the model's result in the wet season (continue).

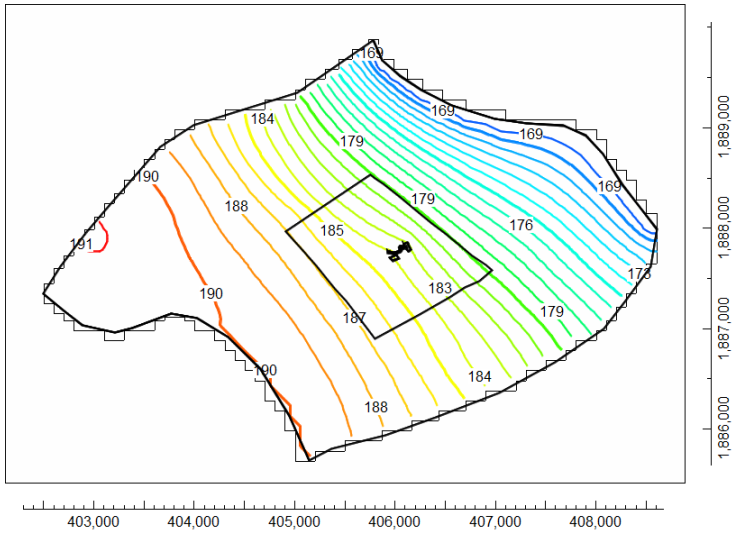


**Figure 26** A new boundary was established using the water table from the model's results.

## 3.3 Particular Area Model Setup

### 3.3.1 Boundary Conditions

The water table at levels 180 and 187 m.a.s.l. was defined as the constant head (CHD Package), and the flow lines were defined as no-flow boundaries.

### 3.3.2 Grid Design

In the simulation, the study area has been divided into grid cells measuring 10 by 10 meters. This division consists of 189 columns extending in the east-west direction and 156 rows in the north-south orientation, leading to a cumulative total of 43,412 grid cells distributed among three layers of groundwater. Figure 27 depicts the grid layout for the study area. This structured arrangement of grid cells aims to enhance precise and efficient computations during the simulation process.

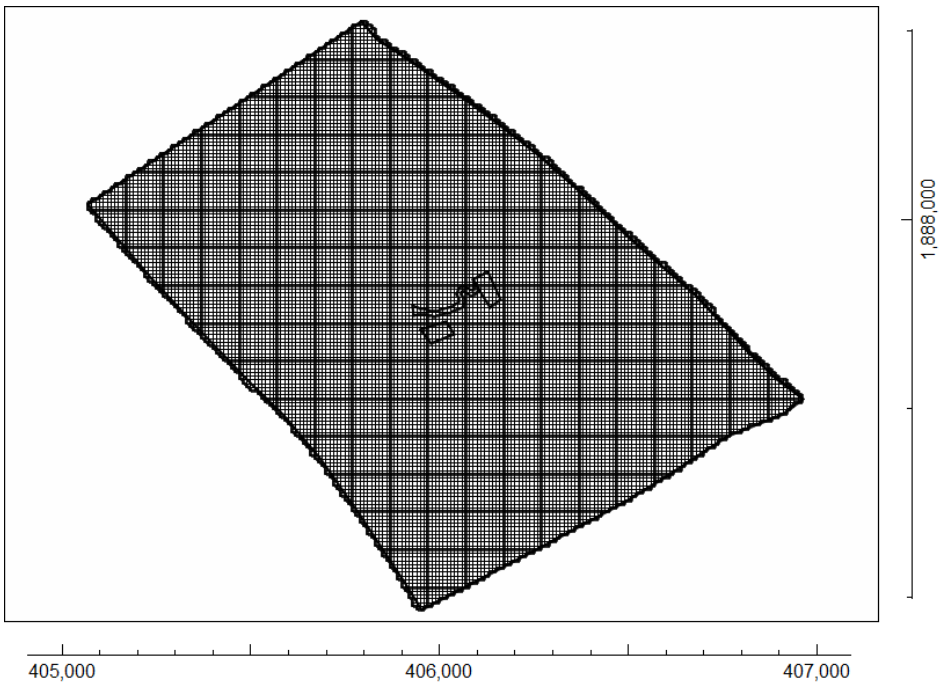


**Figure 27** Grid division for the study area.

### 3.3.3 Model Package Setup

The hydraulic conductivity ($K_H$ and $K_V$), recharge rate (RCH Package), evapotranspiration rate (EVT Package), and hydraulic head observation (OBS Package) were set to the same as the adjusted model.

# 4. RESULT

## 4.1 Model Calibration

The water levels from 9 wells were used to calibrate the model results in two scenarios, before and after the construction of the MAR system. The measured water levels from June 2021 were utilised to calibrate the model prior to the establishment of the MAR, while the water levels from June 2022 were used for calibration after the MAR was constructed.

The calibration results in both scenarios indicate a strong alignment between the simulated and observed heads. The RMSR was 0.56 m before constructing the MAR and 0.24 m after constructing the MAR. Figures 28 and 29 illustrate the calibration graph between the simulated and observed heads of both scenarios.

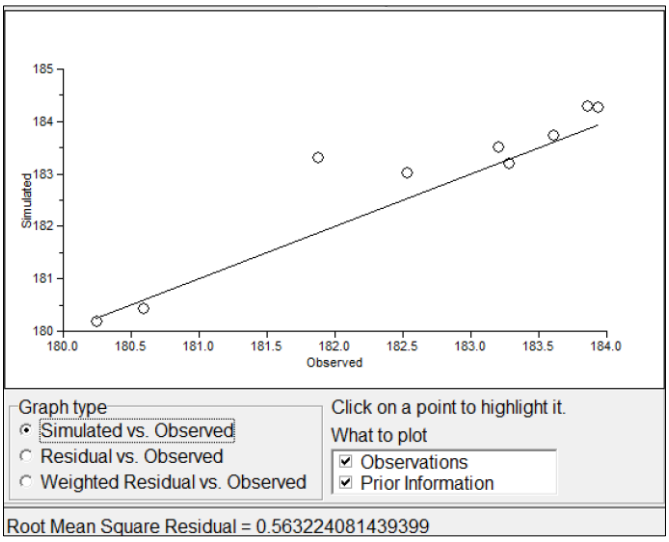


**Figure 28** Simulated head vs observation head and RMSR before constructing the MAR.

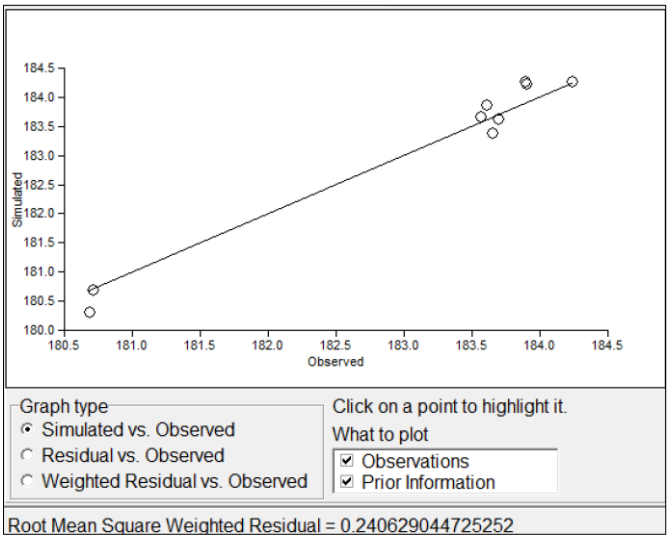


**Figure 29** Simulated head vs observation head and RMSR after constructing the MAR.

## 4.2 Hydraulic head distribution and Comparison

### 4.2.1 Hydraulic head distribution

The hydraulic head is a crucial indicator of groundwater movement, showing a general flow direction from the southwest toward the northeast (Figure 30). This pattern not only aligns with theoretical expectations but also reflects the real-world flow dynamics observed in the field.

### 4.2.2 Hydraulic head comparison

This study aims to compare the hydraulic head under two scenarios in the next ten years, without and with MAR. The analysis involves two distinct seasons, the wet season and the dry season.

**1) Wet Season**

The hydraulic head of both scenarios did not indicate a significant difference. However, the hydraulic head of this season is greater than that of the dry season (Figure 30).

**2) Dry Season**

There is a significant difference in hydraulic head between the two scenarios. The hydraulic head simulated with MAR, both near the MAR and along the flow direction, is higher than the head simulated without MAR, as explained in Figure 30.

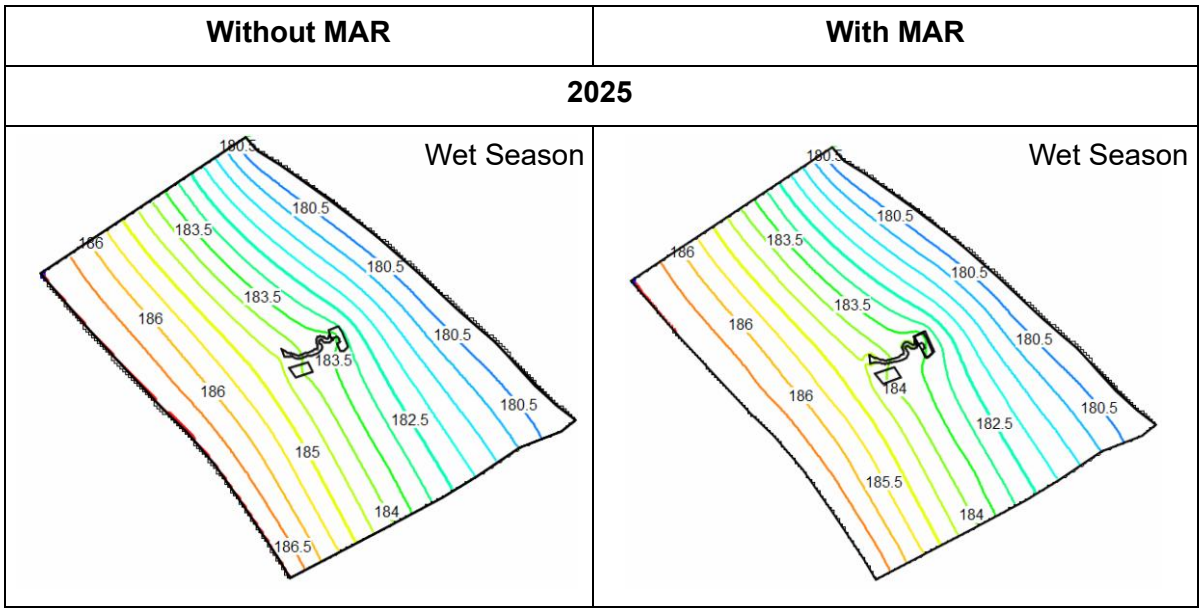


**Figure 30** Water table contour in the wet and dry seasons (m.a.s.l).

| Without MAR | With MAR |
|---|---|
| **2025 (continue)** | |
| 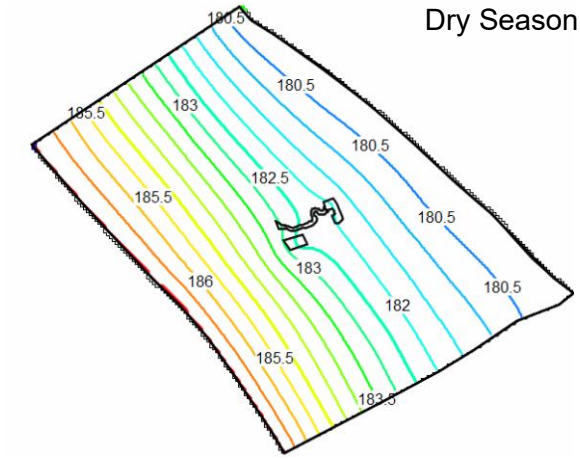  | 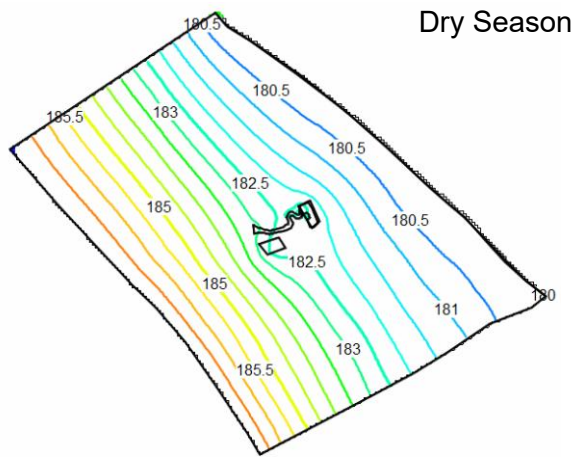  |
| **2026** | |
| 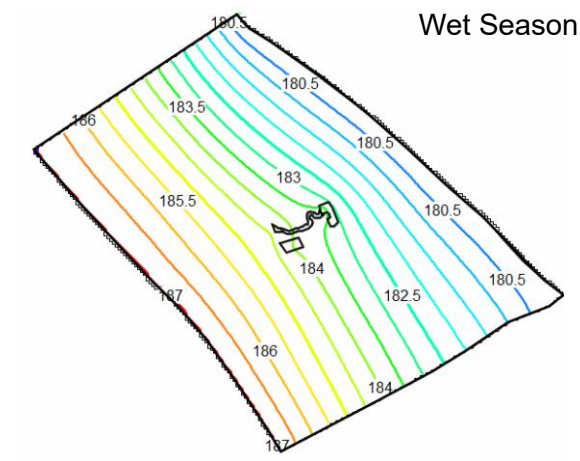  | 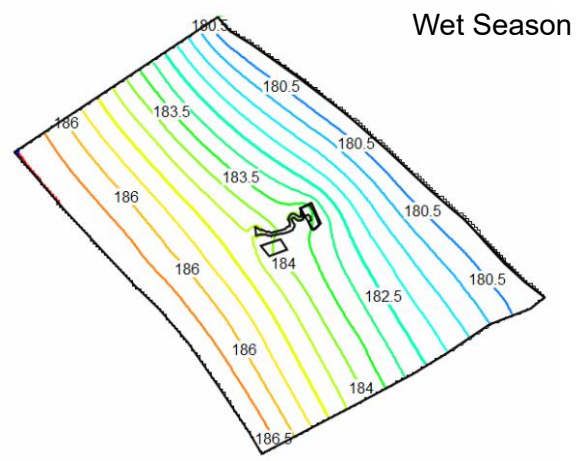  |
| 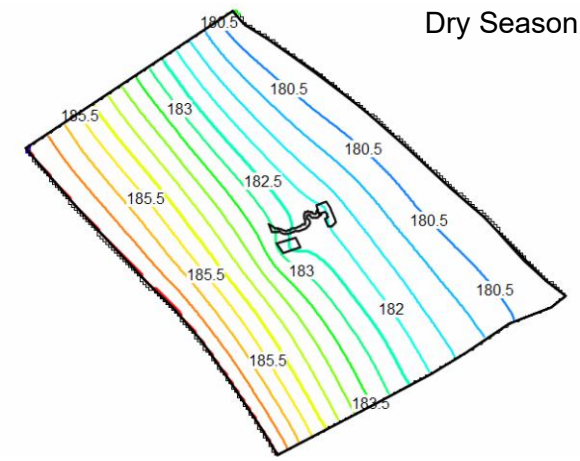  | 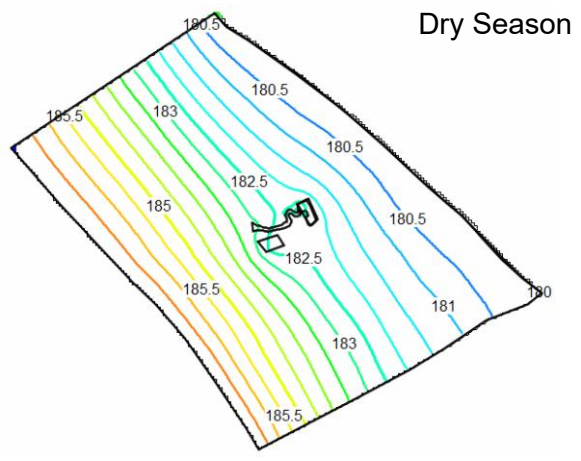  |

**Figure 30** Water table contour in the wet and dry seasons (m.a.s.l) (continue).

| Without MAR | With MAR |
|---|---|
| **2027** | |
| 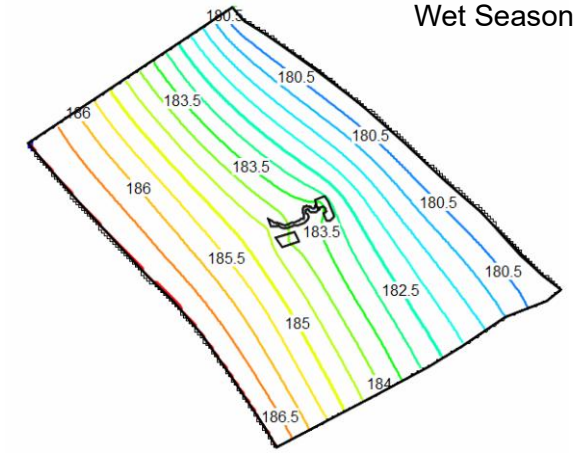  | 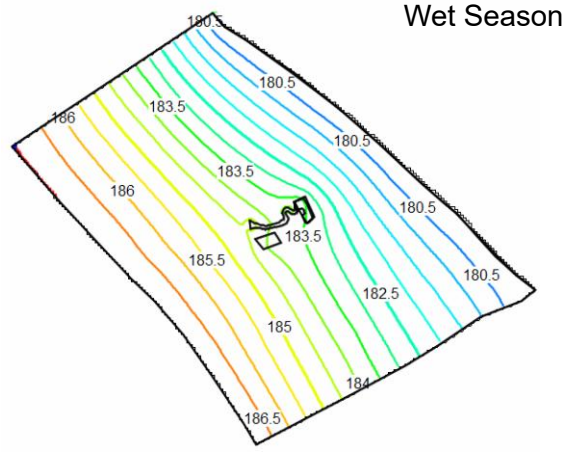  |
| 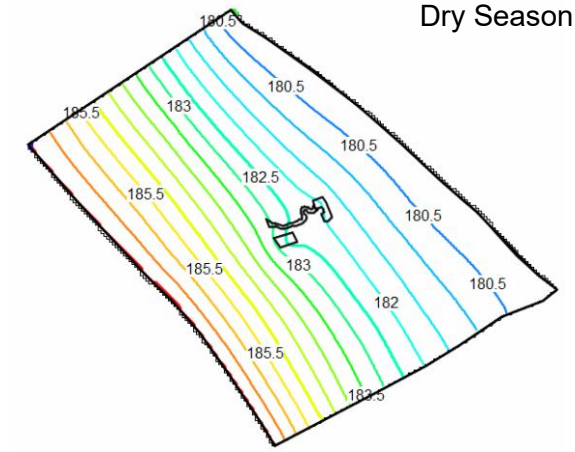  | 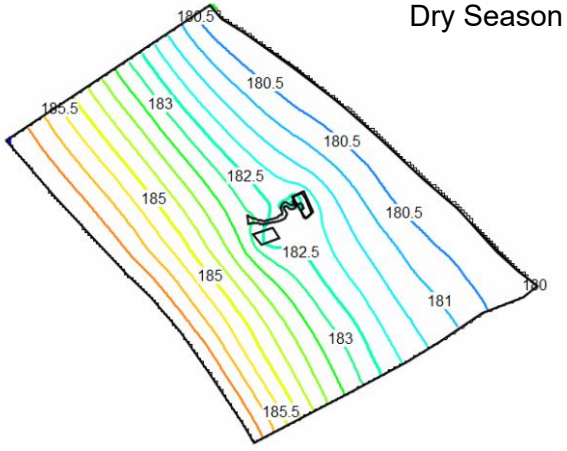  |
| **2028** | |
| 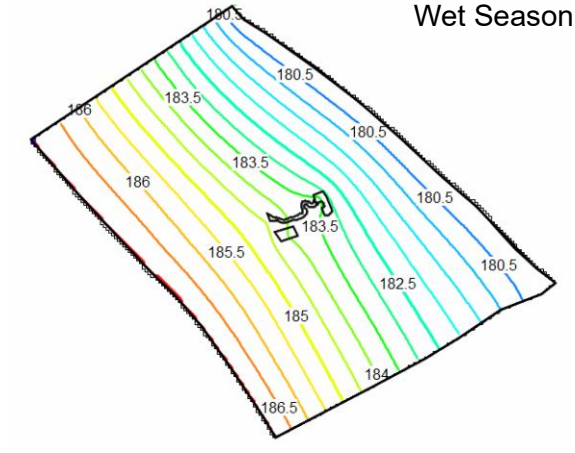  | 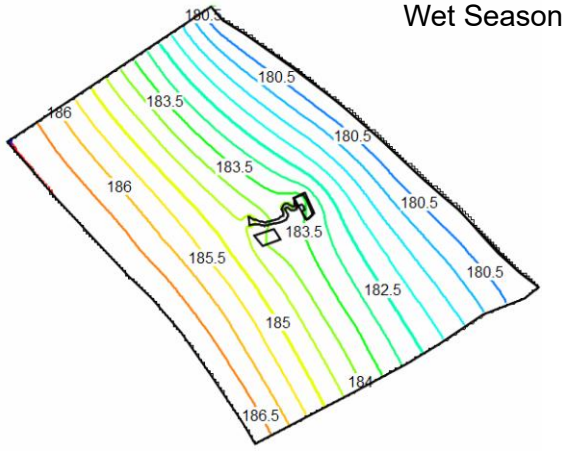  |

**Figure 30** Water table contour in the wet and dry seasons (m.a.s.l) (continue).

| Without MAR | With MAR |
|---|---|
| **2028 (continue)** | |
| 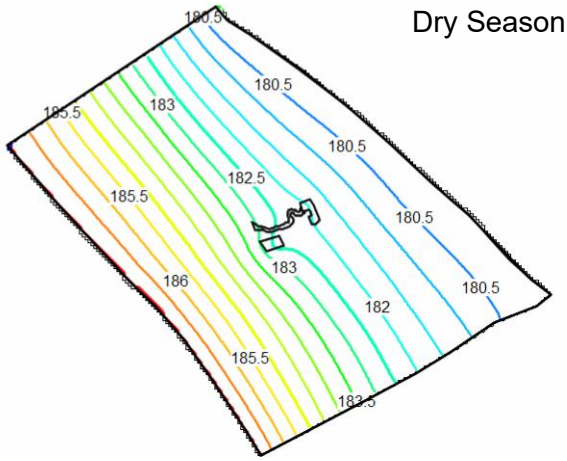  | 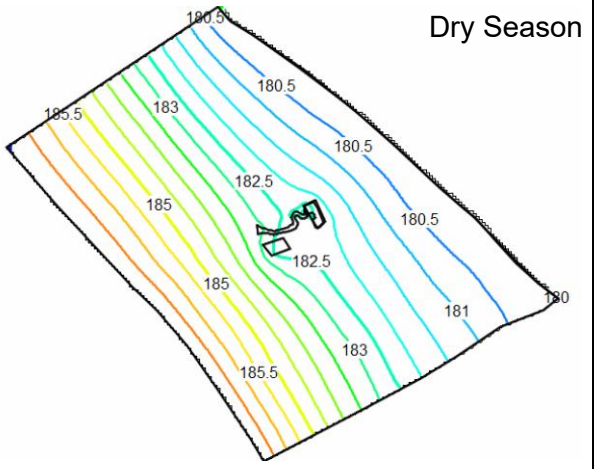  |
| **2029** | |
| 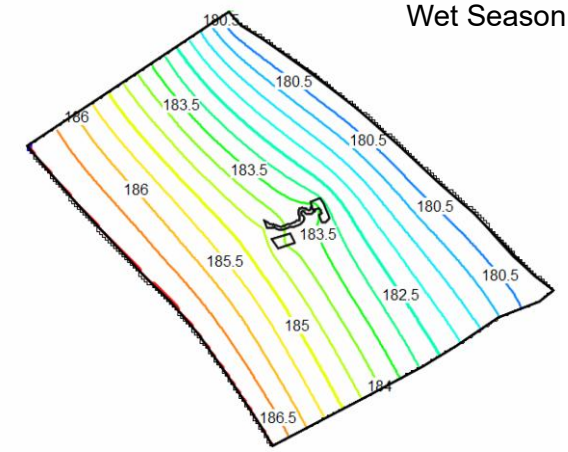  | 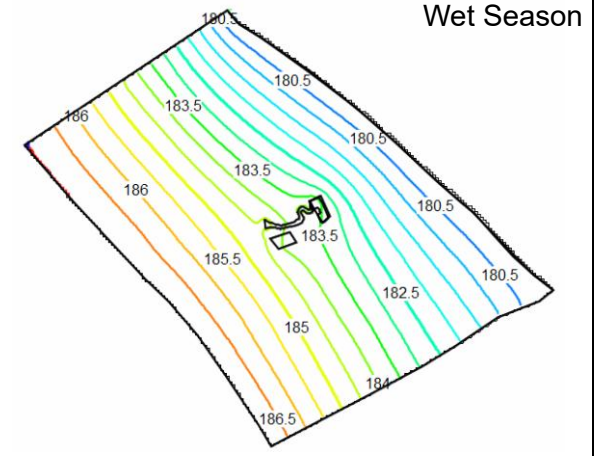  |
| 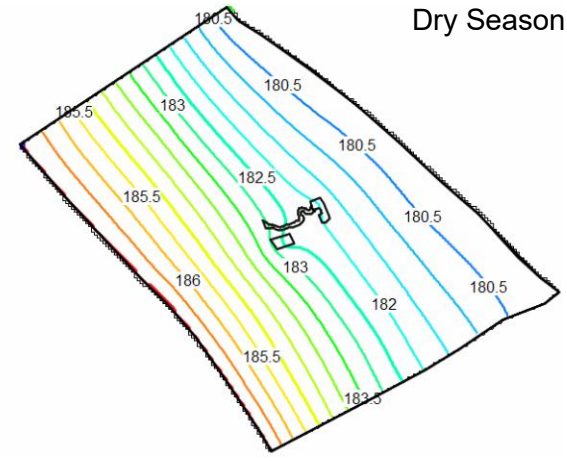  | 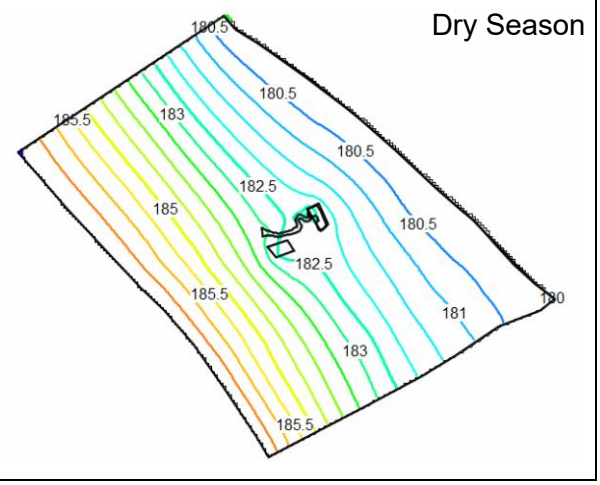  |

**Figure 30** Water table contour in the wet and dry seasons (m.a.s.l) (continue).

| Without MAR | With MAR |
|---|---|
| **2031** | |
| 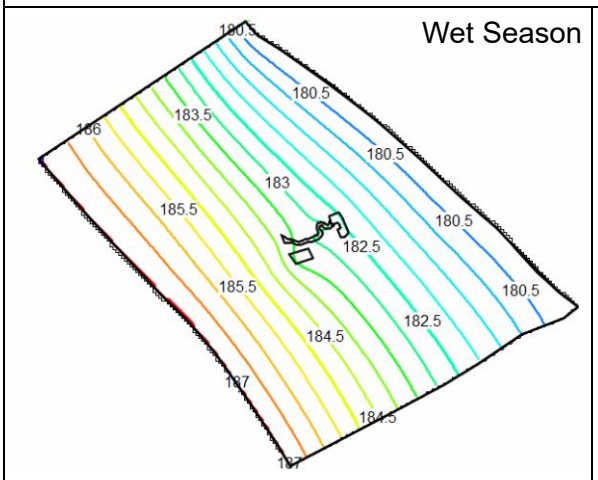  | 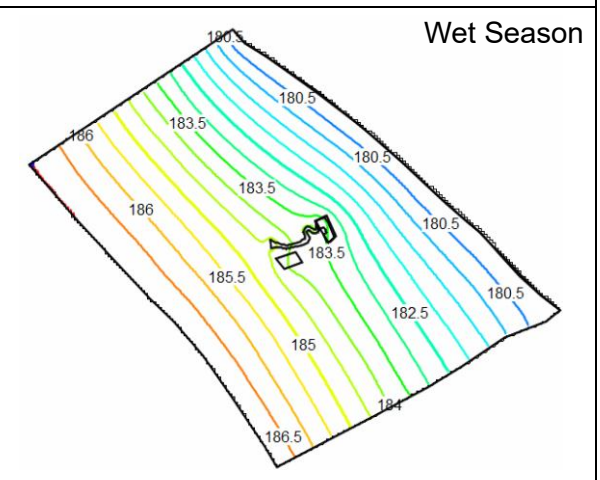  |
| 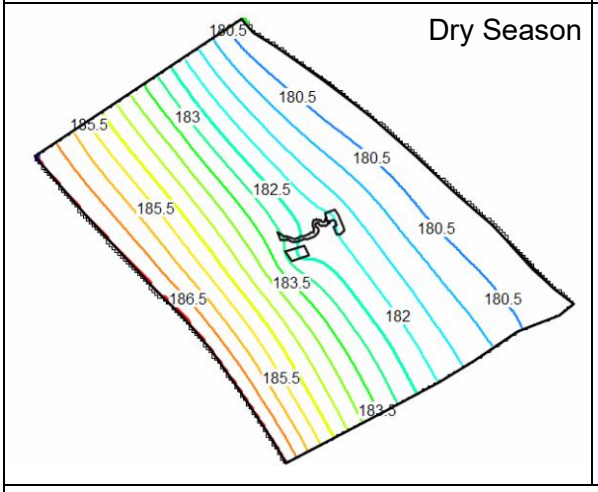  | 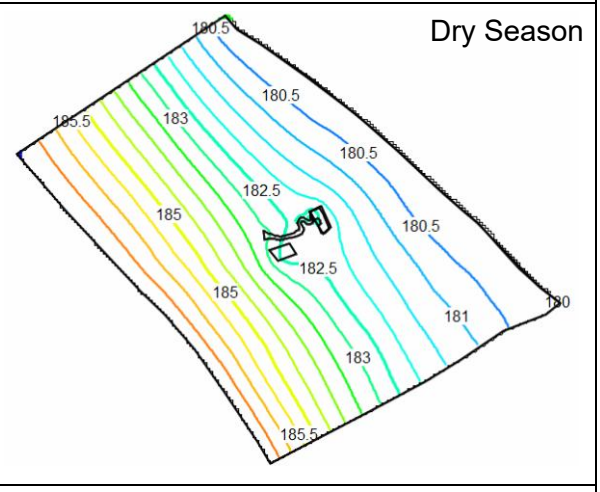  |
| **2034** | |
| 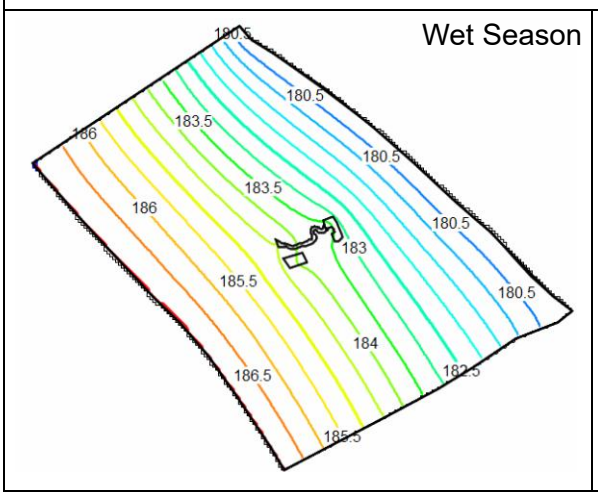  | 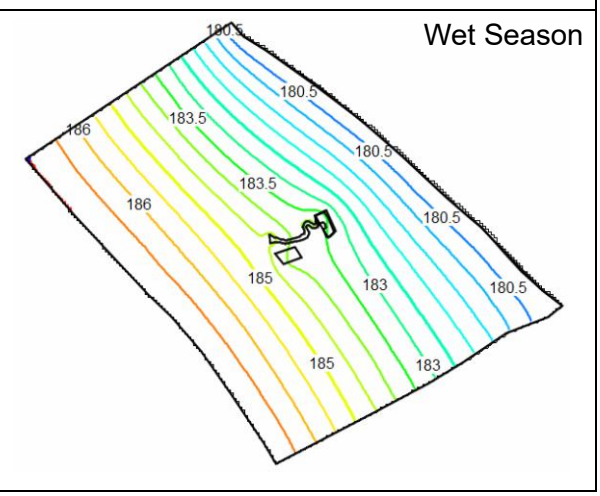  |

**Figure 30** Water table contour in the wet and dry seasons (m.a.s.l) (continue).

| Without MAR | With MAR |
|---|---|
| **2034 (continue)** | |
| Dry Season | Dry Season |

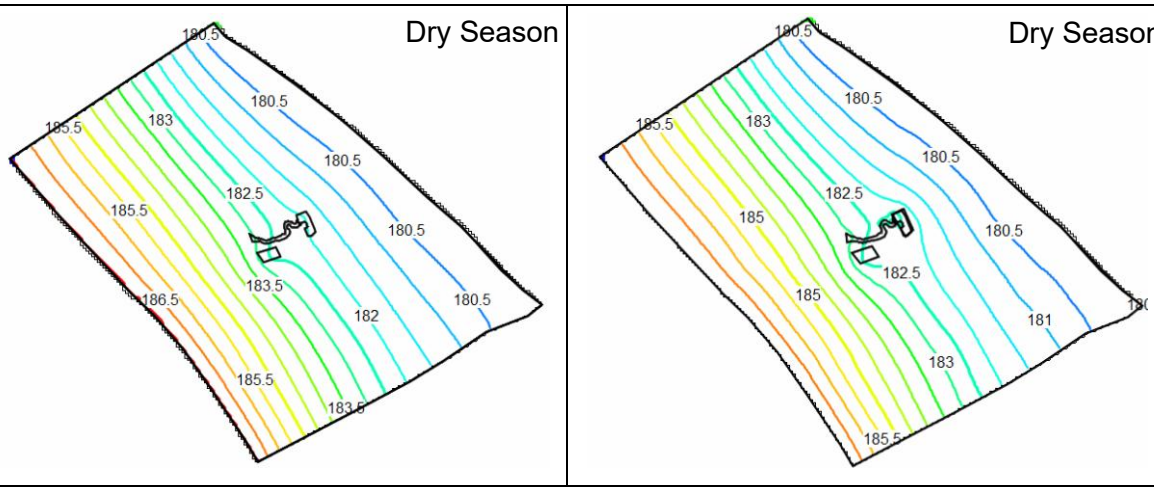


**Figure 30** Water table contour in the wet and dry seasons (m.a.s.l) (continue).

The head difference is illustrated using the Color Grid tool, as demonstrated in Figure 31. The rainbow colour scheme represents the variation in the water table with MAR in comparison to the scenario without MAR. This difference is determined by subtracting the water level with MAR from the water level without it. The findings indicate that the water table difference along the flow direction from the MAR is greater than zero, as evidenced by the colour gradient that transitions from green to red.

Consequently, constructing MAR significantly improves the water table of the study area, achieving a maximum increase of 0.572 m. However, there are some areas where the water table decreases because evapotranspiration is higher than precipitation.

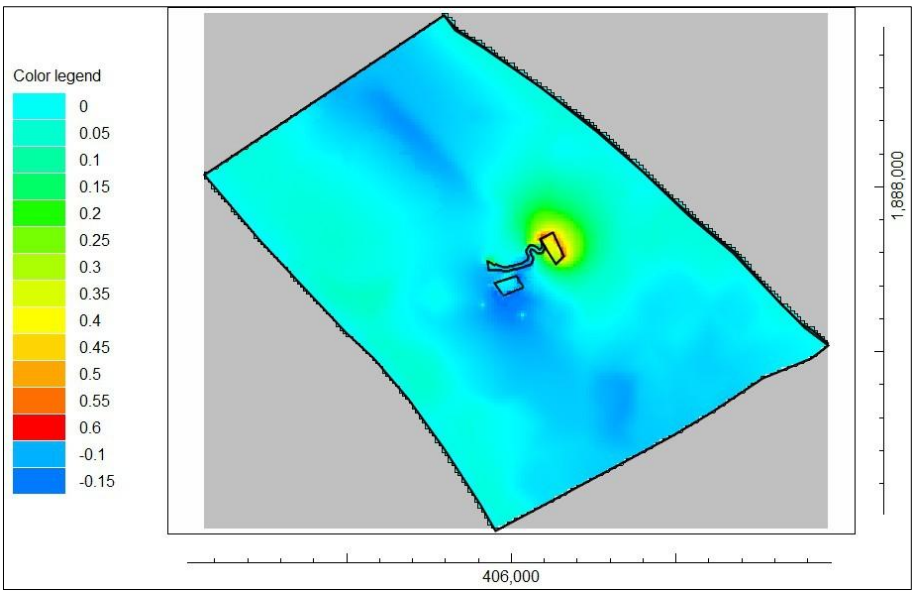


**Figure 31** Head difference between with and without MAR.

## 4.3 Water Budget

ZONEBUDGET was utilised to estimate the amount of water contributed to the aquifer. The MAR was divided into three zones, including Zone 1 (the reservoir), Zone 2 (the sediment basin), and Zone 3 (the canal).

### 4.3.1 Water Budget With MAR

Table 19 indicates that the total volume of water recharged to the aquifer via MAR is estimated at 7.37 Mm³, with a discharge of 6.49 Mm³. The resulting water budget is 0.88 Mm³, available for supporting residents' water needs.

### 4.3.2 Water Budget Without MAR

Table 19 shows that by 2034, the total water volume added to the aquifer through MAR will be 3.40 Mm³, while water discharge via MAR will be 3.48 Mm³. This results in a water budget of -0.07 Mm³, indicating the aquifer system is under stress.

**Table 18** The volume of water recharged to the aquifer ($m^3$).

| | Zone | In | Out | Water budget |
|---|---|---|---|---|
| **With MAR** | Reservoir | 5,358,264.55 | 1,601,056.97 | 3,757,207.57 |
| | Sediment basin | 764,667.19 | 4,204,119.85 | -3,439,452.66 |
| | Canal | 1,247,988.94 | 686,856.57 | 561,132.38 |
| | **Total** | **7,370,920.68** | **6,492,033.39** | **878,887.29** |
| **Without MAR** | Reservoir | 1,468,829.59 | 152,178.57 | 1,316,651.02 |
| | Sediment basin | 168,754.37 | 2,805,991.60 | -2,637,237.23 |
| | Canal | 1,769,901.04 | 521,314.37 | 1,248,586.67 |
| | **Total** | **3,407,485.01** | **3,479,484.54** | **-71,999.54** |

The recharge of water with MAR is 0.95 $Mm^3$ greater than without MAR, resulting in an increase in water levels.

## 4.4 Travel Time and Area Influenced by MAR

### 4.4.1 Travel Time

The travel times were estimated using the MODPATH Package version 7. The Output Mode was set up as Pathlines+Time series, and the Tracking direction was selected as forwards. Table 20 illustrates information on how to set up the MODPATH Package.

**Table 19** The MODPATH Package setup.

| Package | Feature | Setup as | Unit |
|---|---|---|---|
| MODPATH (Winston, 2024) | Output mode (Simulation Type) | Pathlines + Time series | - |
| | Tracking direction | Forwards | - |
| | End of particle tracking (StopOption) | Stop at beginning or end of simulation (1) | - |
| | Initial particle placement | Grid | - |
| | Number of rows in X direction | 20 | - |

Corresponding to Figure 32, the maximum distance that water can travel from the MAR is approximately 2,700 m over a span of ten years. It is important to note that this measurement pertains to horizontal movement only. However, since water also moves vertically, the actual distance travelled may exceed this estimate.

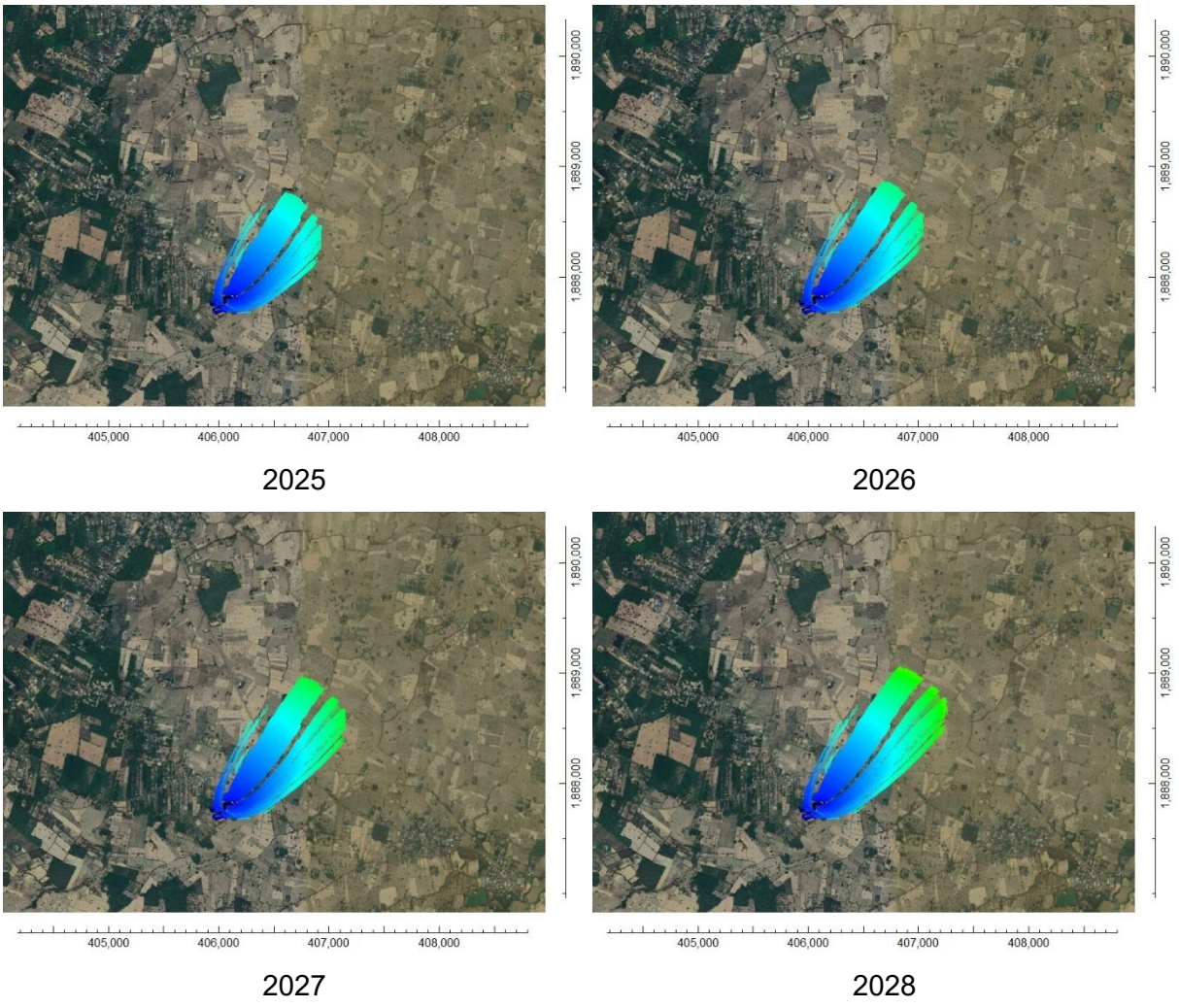


**Figure 32** The distance that water travels from the MAR in different years.

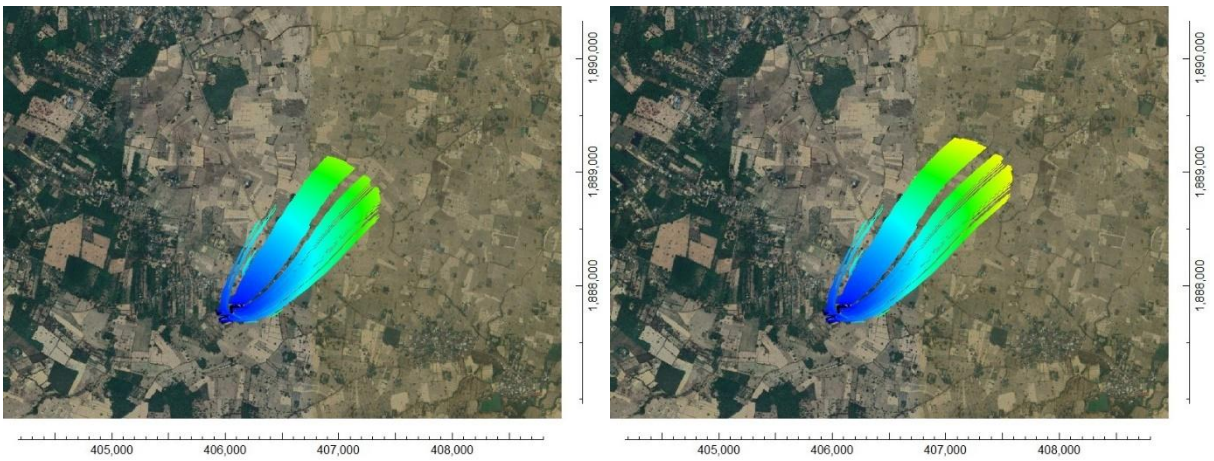


2029 2031

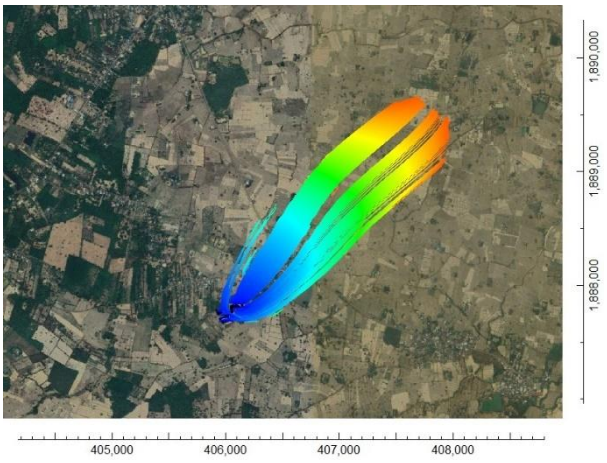


2034

**Figure 32** The distance that water travels from the MAR in different years (continue).

### 4.4.2 Area Influenced by MAR

To estimate the area influenced by the MAR, it is essential to activate the MODPATH to assess the flow direction. The MODPATH package was configured as detailed in Table 20, and the path line is depicted in Figure 32. The area influenced by MAR was determined by drawing a polygon around the path line, resulting in an estimated area of approximately 1.3 km².

The area impacted by the MAR contains two groundwater extraction wells. The operation of these wells significantly influences the dynamics of groundwater flow, as illustrated in Figure 33.

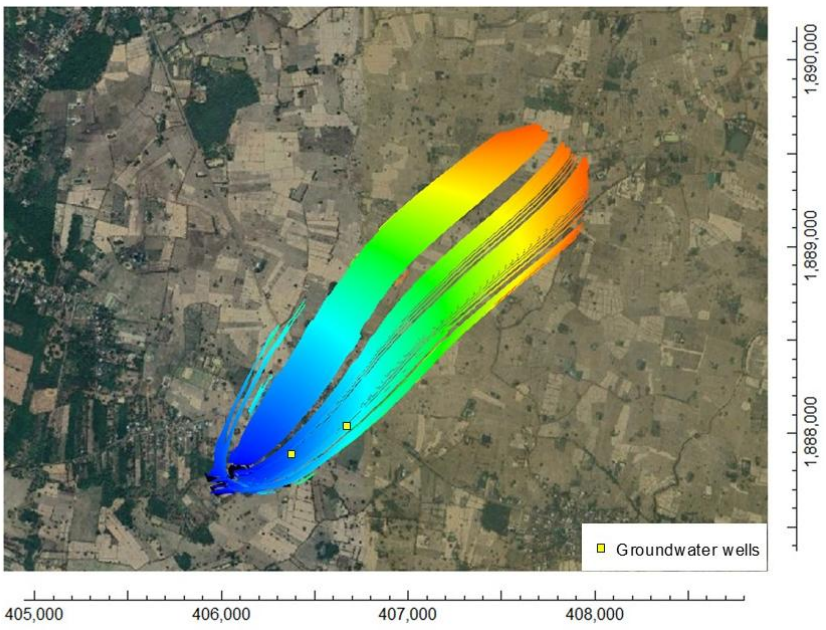


**Figure 33** The groundwater flow is affected by water extraction.

## 4.5 Advantages for the local population

The farmers living downstream (personal communication, 24 September 2024) reported that before the construction of the MAR, they were unable to extract groundwater during the five-month dry season, January to May. After establishing the MAR, it was beneficial for their wells, enabling them to extract groundwater throughout the year.

According to 2.5 water use, 2,462 $m^3$ per month of groundwater was extracted to serve as a primary source of water for a population of 684. This means that, prior to MAR, groundwater was extracted for a total of 7 months, resulting in an annual extraction of 17,234 $m^3$. Following MAR, the annual extraction of groundwater amounts to 29,544 $m^3$. The availability of water in volumes exceeding 12,310 $m^3$ is particularly beneficial for consumption, and over 72,190 $m^3$ per year is still accessible for agriculture during the dry season.

# 5. DISCUSSION

This study analysed the effectiveness of the MAR system implemented by the DGR in Dong Khwang village, Sakon Nakhon Province, using a combination of field data, hydrogeological analysis, and numerical modelling through MODFLOW in ModelMuse. The primary focus was to estimate the groundwater level with and without constructing the MAR, estimate water levels of two scenarios, and compare the hydraulic head of the two scenarios during the wet and dry seasons.

## 5.1 Groundwater level

The simulation results indicate a significant difference in groundwater levels between the scenarios with and without the MAR, particularly during the dry season. In the dry season, the hydraulic head showed a notable increase under the MAR scenario, the greatest increase of 0.572 m, 0.57 m greater than without MAR (see Figure 31). During the wet season, both scenarios exhibited similar groundwater levels (Figure 30).

## 5.2 Groundwater recharge

The simulation indicated that the water budget increases over the next ten years with 0.88 $Mm^3$ with the MAR system, compared to a reduction in resources of -0.07 $Mm^3$ for the case without the MAR system. This suggests that MAR plays a significant role in recharging water to the aquifer. Additionally, the recharge calculations using water balance demonstrate the system's efficiency. The natural recharge rate in the area is approximately 11.33% of rainfall, whereas the MAR system achieved a notably higher rate of 19.81%. This increase is probably due to improved infiltration within the system, which aligns with the model results and confirms that the MAR system can effectively raise the water levels in the study area.

## 5.3 Travel Time and Area Affected by MAR

The travel time and the area affected by the MAR were estimated by MODPATH. The simulation demonstrates that, by 2034, the water could travel a maximum of approximately 2,700 m. horizontally. The MAR affected area was around 1.3 $km^2$. This illustrates the extended spatial and temporal effects of the MAR intervention on local groundwater systems.

## 5.4 Model Calibration

The model calibration validated that there is a good fit between the simulated head and the observed head after parameter adjustment, particularly hydraulic conductivity. This confirms the model's capacity to represent actual conditions (Winston, 2019). These findings are consistent with prior studies suggesting MAR as a sustainable method for groundwater replenishment in semi-arid and drought-prone regions (Dillon, 2021).

## 5.5 Limitation

The model does have limitations. For example, the hydraulic conductivity measured by the slug test, the boundary condition, and the hydraulic head observation.

### 5.5.1 Hydraulic conductivity

The hydraulic conductivity was measured using the slug test, which can sometimes underestimate actual values. Additionally, the measurements were taken from observation wells located near the MAR system. As a result, the data reflects the hydraulic conductivity in that specific area, which may not be very efficient for the whole area. Another method, such as a pump test, could be used to measure the hydraulic conductivity in additional wells located throughout the study area.

### 5.5.2 Boundary Condition

**1) Constant Head Boundary**

The study area lacks a mountain or a primary river. Consequently, the model boundary was established based on the equipotential line and designated as a constant head boundary. Additionally, the flow direction was designated as a no-flow boundary. This arrangement may lead to errors in the model's results.

**2) Recharge Rate**

The recharge rate was determined by analysing rainfall, evapotranspiration, and changes in surface water levels. Surface runoff data were lacking, which is a limitation of the study. Therefore, alternative methods such as the Chloride Mass Balance (CMB) method, the Water Table Fluctuation (WTF) method, and the soil infiltration test can be utilised for this calculation. By comparing the results obtained from these various methods, this can effectively minimise discrepancies in the estimated recharge rate. Because even a slight deviation in input data can affect model output (Allen et al., 1998).

This simulation did not account for the clogging, which can reduce the recharge to the aquifer. A study conducted by Hutchison et al. (2013) suggests that blocking the infiltration surface and the resulting decrease in infiltration rates pose significant challenges for all artificial recharge systems. This issue is particularly concerning in surface spreading facilities, where the presence of suspended solids and microorganisms in the recharge water can lead to significant clogging over time.

**3) Water Level Data**

There is only one year of water level data available for the MAR system. The water levels were measured in 2022 (Table 6), following the establishment of the MAR. Gathering data for more than one year would enhance the model's results. For example, the water level data can be used to calculate the recharge rate and can also serve as valuable input for the River Package.

### 5.5.3 Future Projection

The projections for rainfall and evapotranspiration trends are derived from linear regressions, which may not completely capture the complexities of climate dynamics (Wolberg, 2006). As climate patterns change, the long-term predictive accuracy of the model could diminish. Therefore, the model should be continuously updated as new data becomes available.

# 6. CONCLUSION AND RECOMMENDATION

## 6.1 Conclusion

This study demonstrates that the MAR system, established in December 2022 in Dong Khwang village, Sakon Nakhon Province, Northeastern Thailand, significantly improves groundwater availability, particularly during dry seasons. This development is achieved through both natural and artificial recharge methods. By integrating field data with GIS mapping, it was observed that groundwater flows from the southwest to the northeast. Additionally, MODFLOW simulations provided a thorough assessment of the hydrological dynamics in the region. The MAR system increased recharge from -0.07 $Mm^3$ to 0.88 $Mm^3$, resulting in a rise in groundwater levels, with a maximum increase of 0.57 m.

According to the parameter's adjustment, hydraulic conductivity ($K_H$) is identified as the most sensitive parameter. In the first simulation, the $K_H$ values were obtained from the slug test measurement. Subsequently, these values were adjusted to achieve the minimum RMSR. The middle layer had the most significant increase in hydraulic conductivity, increasing by 51 times. Followed by the hydraulic conductivity of the upper unconfined aquifer and the lower layer, which rises 3 and 2.3 times, respectively. Consequently, the $K_H$ values were adjusted to 27.693 m/d for the middle layer (up from 0.543 m/d), 1.5 m/d for the upper unconfined aquifer (up from 0.5 m/d), and 0.878 m/d for the lower layer (up from 0.382 m/d). Overall, the RMSR improved significantly, dropping from 4.99 to 0.49 m.

The study also highlighted that the local population could extract 12,310 $m^3$/year of water during the dry period, potentially supporting the domestic and agricultural water needs of 684 residents. The influence of MAR extends beyond recharge zones, affecting groundwater movement over an area of up to 1.3 $km^2$, with a travel distance of 2,700 m. These insights can be applied to the suitability of rural water management initiatives across Thailand and similar contexts.

This study presents a scientifically grounded approach to support the use of MAR systems as an adaptive strategy for addressing future water shortages caused by climate change. The findings also support the importance of integrating hydrological modelling in water management planning and policy support.

## 6.2 Recommendations

### 6.2.1 Monitoring and Evaluation

Due to the ongoing need to develop groundwater models, continuous long-term monthly monitoring of groundwater levels, surface water levels, precipitation, evapotranspiration, and water quality remains essential. Furthermore, to ensure the water resource maintains high quality before recharging into the aquifer, water quality should be monitored, especially since this area is mainly used for agriculture.

### 6.2.2 Expansion of MAR Systems

This study analysed the experimental project to recharge groundwater aquifers with surface water operated by the DGR. The result can be considered for implementing similar systems in other drought-prone areas, using the Dong Khwang model as a reference.

### 6.2.3 Public Awareness and Training

This is a long-term simulation, so system maintenance is a significant problem. Therefore, it is essential to provide training for local stakeholders on groundwater management, system maintenance, and water conservation.

### 6.2.4 Model Refinement

Update the model periodically with new data to increase accuracy and account for changing hydrological conditions and land use patterns.

### 6.2.5 Policy Integration

Integrate MAR planning into local and national water management policies to enhance surface and groundwater management.

In summary, the MAR system not only improves water storage but also establishes a long-term strategy for aquifer sustainability, particularly in regions vulnerable to climatic variability and groundwater depletion. The modelling outcomes and real-world recharge data confirm MAR as a reasonable and impactful intervention for rural groundwater management in Thailand.

# BIBLIOGRAPHY


Allen, R. G., Pereira, L. S., Raes, D. & Smith, M. 1998. Crop evapotranspiration-Guidelines for computing crop water requirements-FAO Irrigation and drainage paper 56. *Fao, Rome,* 300**,** D05109.

Banta, E. R. 2000. MODFLOW-2000, the U.S. Geological Survey Modular Ground-Water Model; documentation of packages for simulating evapotranspiration with a segmented function (ETS1) and drains with return flow (DRT1). *Open-File Report.*

Bovolo, C. I., Parkin, G. & Sophocleous, M. 2009. Groundwater resources, climate and vulnerability. *Environmental Research Letters,* 4**,** 035001.

Butler Jr, J. J. 2019. *The design, performance, and analysis of slug tests*, Crc Press.

Department of Environment, Great Lakes, and Energy 2025, *Groundwater Modeling – Calibration,* Department of Environment, Great Lakes, and Energy, State of Michigan, United State, viewed 5 July 2025, <https://www.michigan.gov/egle/about/organization/remediation-and-redevelopment/groundwater-modeling-overview/groundwater-modeling-calibration>.

Department of Groundwater Resources 2012, *Hydrogeological Map of Northeastern Thailand 1:50,000 Series,* Department of Groundwater Resources, Thailand.

Department of Groundwater Resources 2021, *The potential exploration of groundwater recharge in the Nam Kam basin Project,* Department of Groundwater Resources, Thailand.

Department of Groundwater Resources 2022, *An experimental project to recharge groundwater aquifer with surface water in Nam Kam basin, Sakon Nakhon, Thailand,* Department of Groundwater Resources, Thailand.

Department of Land 2019, *Expropriation and Acquisition of Real Estate Act,* Department of Land, Thailand.

Department of Mineral Resources 2007, *Geology of Thailand*, Department of Mineral Resources, Thailand.

Department of Mineral Resources 2011, *Stratigraphy of the Khorat Group in the upper northeastern region*, Department of Mineral Resources, Thailand.

Department of Provincial Administration 2024, *Population statistics by civil registration*, Department of Provincial Administration, Thailand, viewed 2 January 2025, <https://stat.bora.dopa.go.th /stat /statnew/statMenu/newStat/home.php>.

Dillon, P., Dillon, P., Fernández Escalante, E., Megdal, S. B. & Massmann, G. 2021. *Managed Aquifer Recharge for Water Resilience,* Basel, Switzerland, MDPI - Multidisciplinary Digital Publishing Institute.

East Asia Forum 2020, *Thailand's water shortage and inequality crisis*, East Asia Forum, Australia, viewed 2 November 2024, <https://eastasiaforum.org/2020/03/20/thailands-water-shortage-and-inequality-crisis/>.

Fetter, C. W. 2018. *Applied hydrogeology*, Waveland Press.

Freeze, R. A. 1984. Groundwater contamination. Wiley Online Library.

Freeze, R.A. and Cherry, J.A., 1979. *Groundwater*. Englewood Cliffs, NJ: Prentice-Hall.

Harbaugh, A. W. 2005. *MODFLOW-2005, the US Geological Survey modular ground-water model: the ground-water flow process*, US Department of the Interior, US Geological Survey Reston, VA, USA.

Hughes, J. D., Langevin, C. D. & Banta, E. R. 2017. Documentation for the MODFLOW 6 framework. *Techniques and Methods.* Reston, VA.

Hutchison, A., Milczarek, M. & Banerjee, M. 2013. *Clogging phenomena related to surface water recharge facilities*. Clogging issues associated with managed aquifer recharge methods, 34-49.

Kdm18505_USG, 2022, *SRTM Thailand,* The University of Georgia, United States, viewed 3 December 2024, <https://usg.maps.arcgis.com/home/item.html?id=b6464d46a4684713a8fd8b568fad8c02>.

Land Development Department 2016, *Soil Permeability,* Land Development Department, Thailand.

Land Development Department 2022, *Land use information,* Land Development Department, Thailand, view 15 December 2024, <https://lddcatalog.ldd.go.th/ dataset/ldd_21_01>.

Local Resident, 2024. *Interviewed by the Department of Groundwater Resources*, 24 September.

Meteorological Department 2024, *Meteorological Statistics Data Request System,* Meteorological Department, Thailand, view 2 January 2025, <https://data-service.tmd.go.th/index.php>.

Phuprakit, P. 2024. Model for success in value-added agricultural business case study: Khoknongna Model, Northeastern Region. *UMT Poly Journal,* 21, 115-134.

Scanlon, B. R., Keese, K. E., Flint, A. L., Flint, L. E., Gaye, C. B., Edmunds, W. M. & Simmers, I. 2006. Global synthesis of groundwater recharge in semiarid and arid regions. *Hydrological Processes,* 20**,** 3335-3370.

Statista 2021, *Monthly per capita water consumption in Thailand in 2021, by region*, Statista, Hamburg, viewed 21 January 2025, <https://www.statista.com/ statistics/1173446/thailand-monthly-per-capita-water-consumption-by-region/https://www.statista.com/statistics/1173446/thailand-monthly-per-capita-water-consumption-by-region/>.

Taylor, R. G., Scanlon, B., Döll, P., Rodell, M., Van Beek, R., Wada, Y., Longuevergne, L., Leblanc, M., Famiglietti, J. S. & Edmunds, M. 2013. Ground water and climate change. *Nature climate change,* 3**,** 322-329.

Todd, D. K. & Mays, L. W. 2004. *Groundwater hydrology*, John Wiley & Sons.

Trinet, K. 2008. Study of rock salt geology and hydrogeology, the Lower Nam Kam Irrigation project, Nakorn Panom. *The Kasetsart University Academic Conference*, Bangkok*,* 46, 401- 410.

Winston, R. B. 2019. ModelMuse Version 4: A graphical user interface for MODFLOW 6. *Scientific Investigations Report.* Reston, VA.

Winston, R.B., 2024, ModelMuse version 5.3.1: U.S. Geological Survey Software Release, 17 September 2024

Wolberg, J. 2006. *Data analysis using the method of least squares: extracting the most information from experiments*, Springer Science & Business Media.

World Resources Institute 2025, *Climate Adaptation and Resilience,* World Resources Institute, Washington DC, viewed 4 March 2025, <https://www.wri.org/climate/climate-resilience>.

# APPENDICES

**Appendix A** Monthly precipitation (mm) graph and trendline between 2005 and 2024.

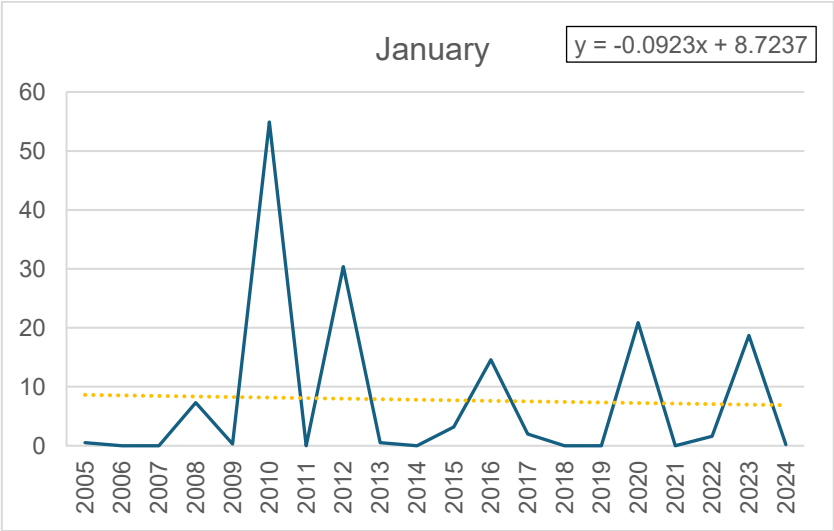


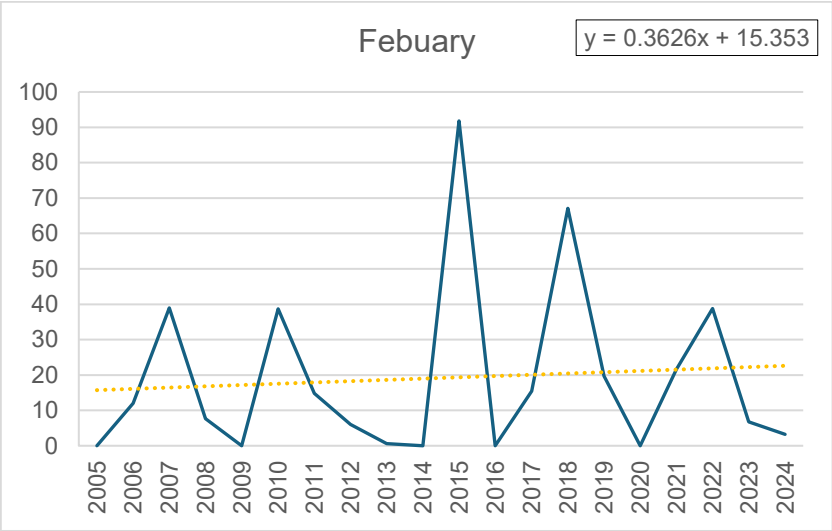


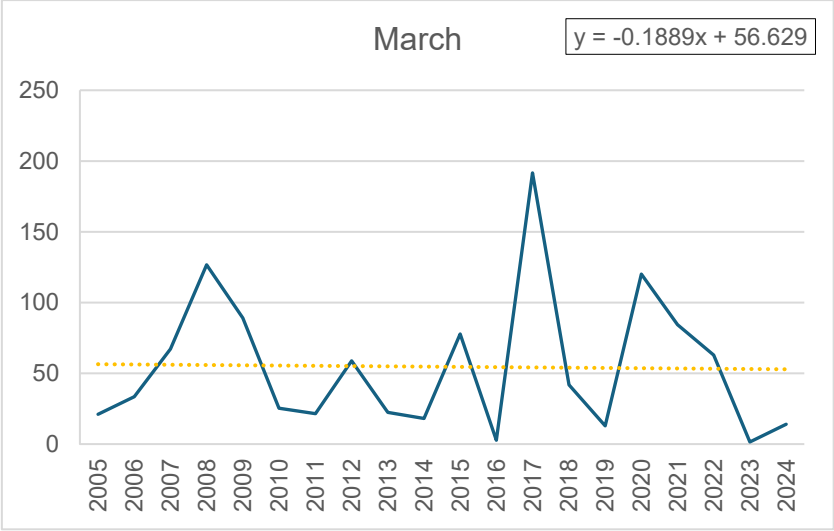


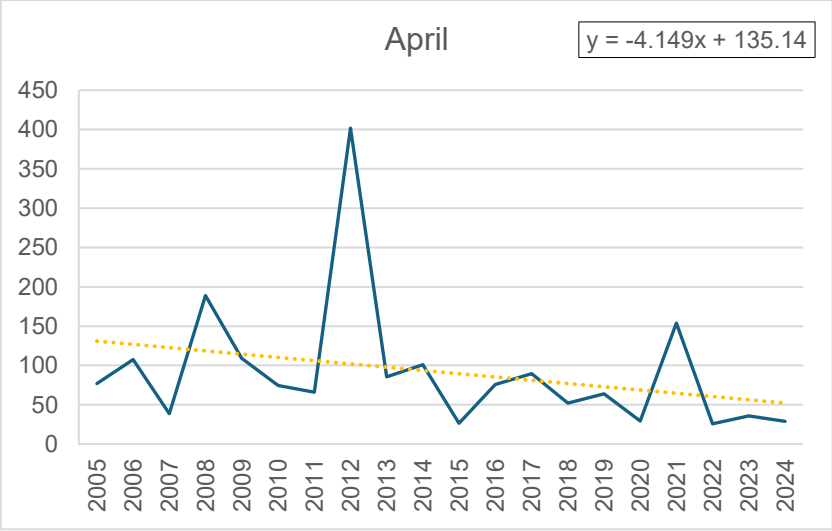

**Appendix A** Monthly precipitation (mm) graph and trendline between 2005 and 2024 (continue).

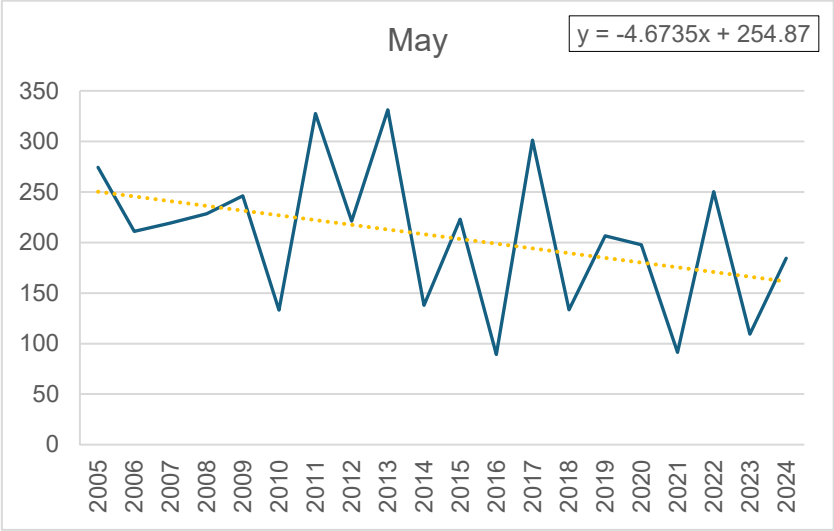


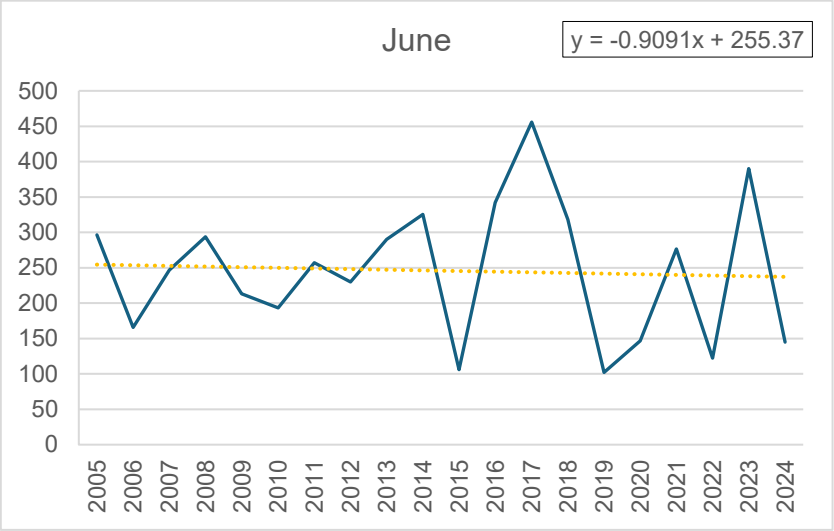


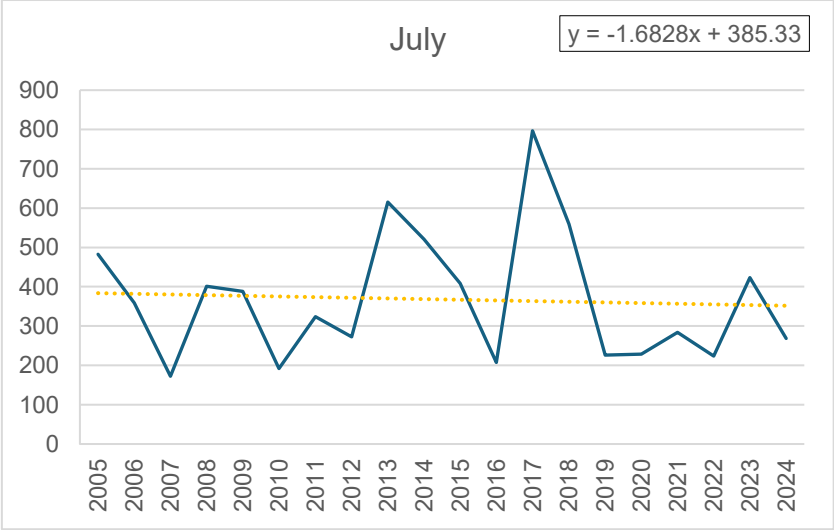


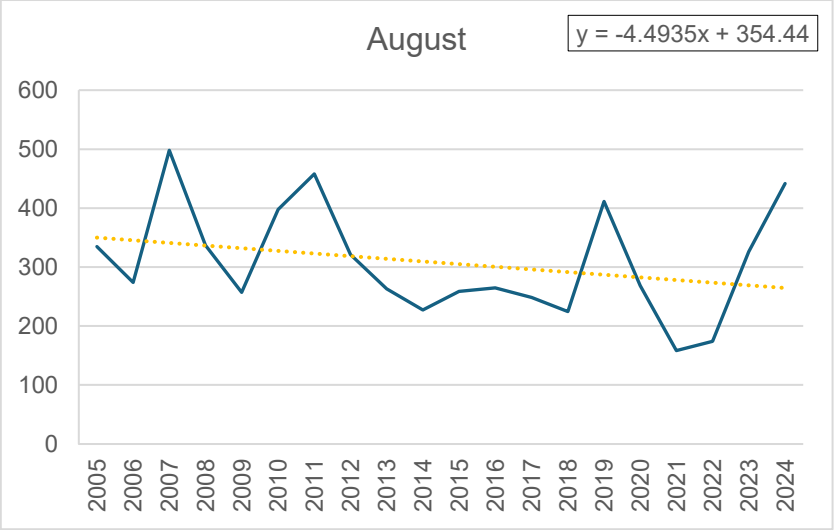

**Appendix A** Monthly precipitation (mm) graph and trendline between 2005 and 2024 (continue).

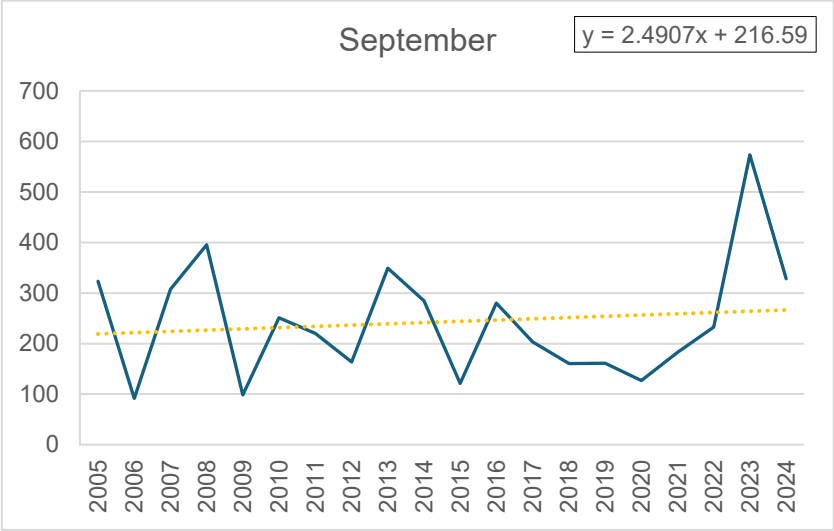


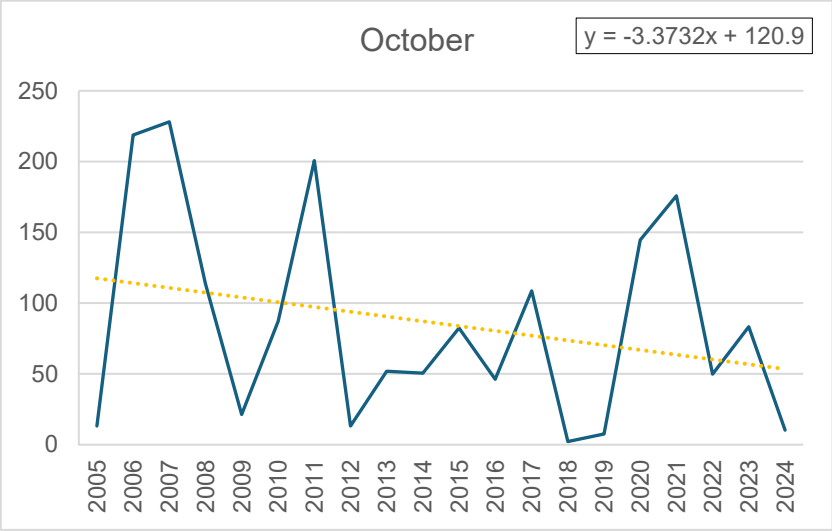


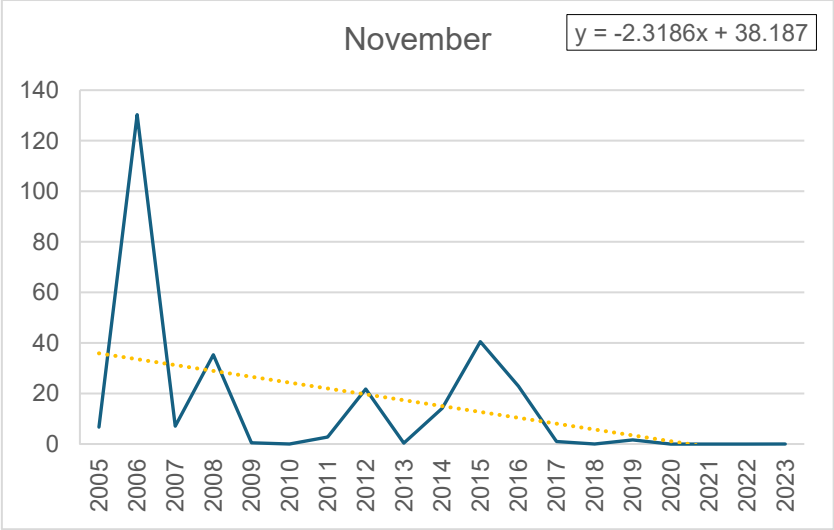


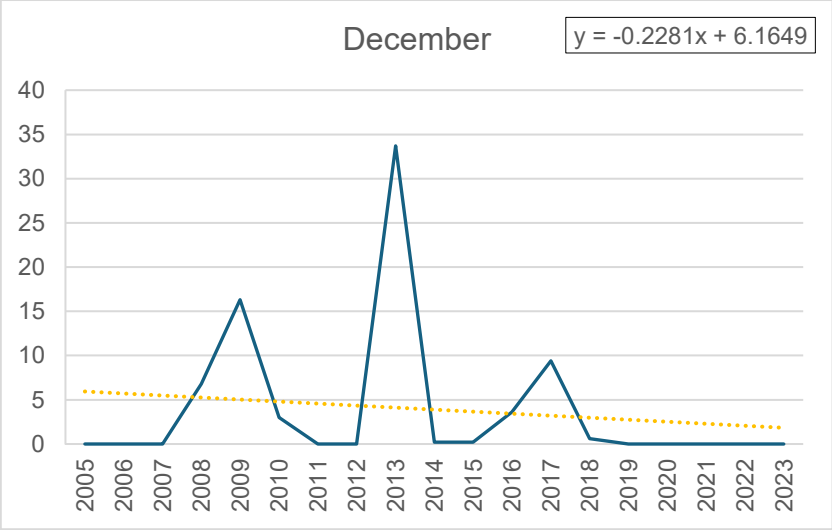

**Appendix B** Monthly evapotranspiration (mm) graph and trendline between 2005 and 2024.

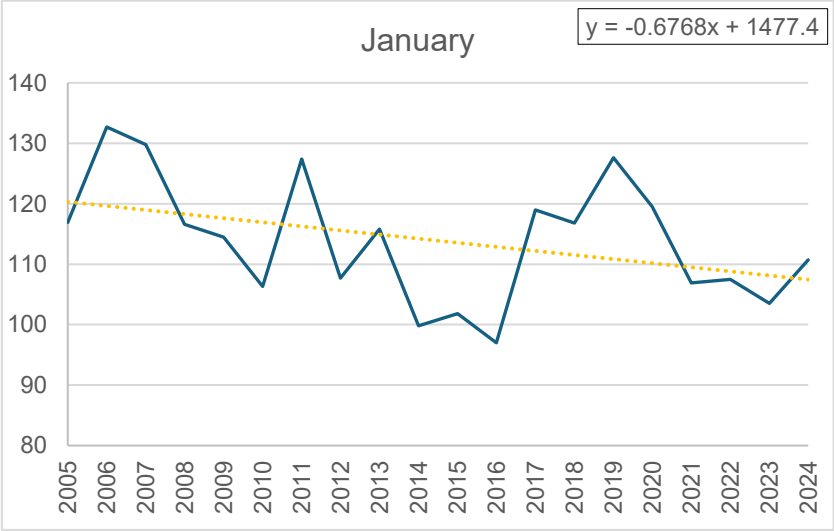


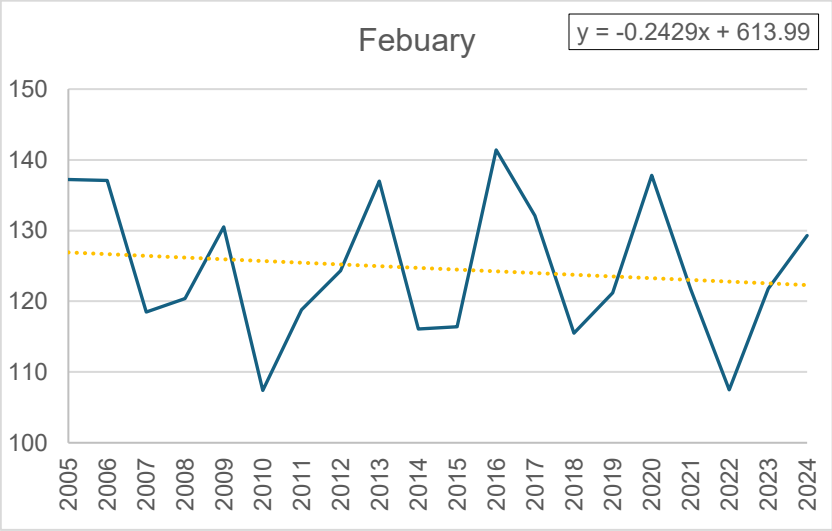


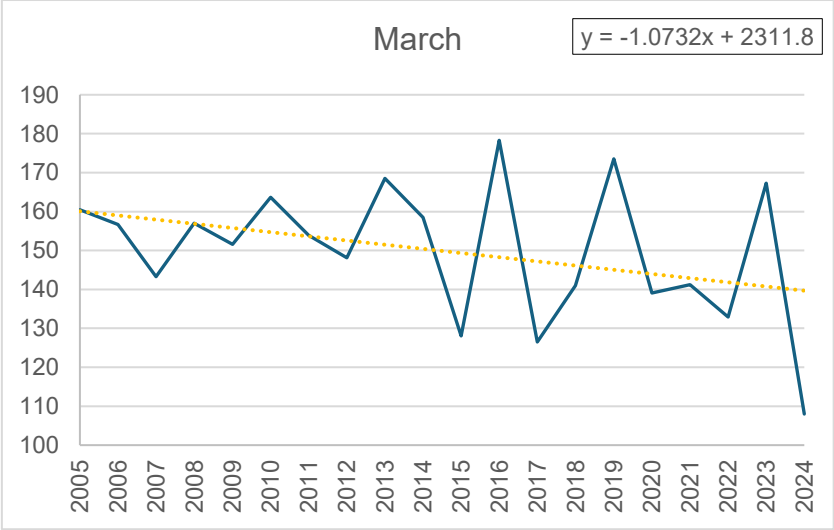


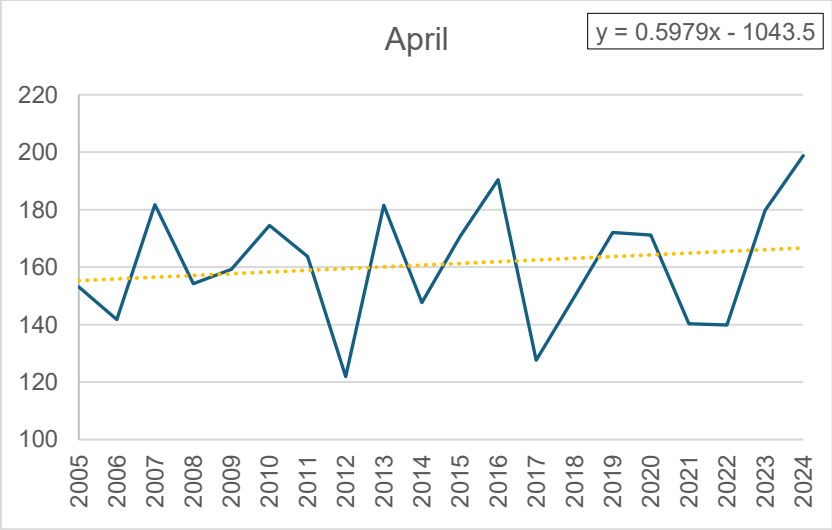

**Appendix B** Monthly evapotranspiration (mm) graph and trendline between 2005 and 2024 (continue).

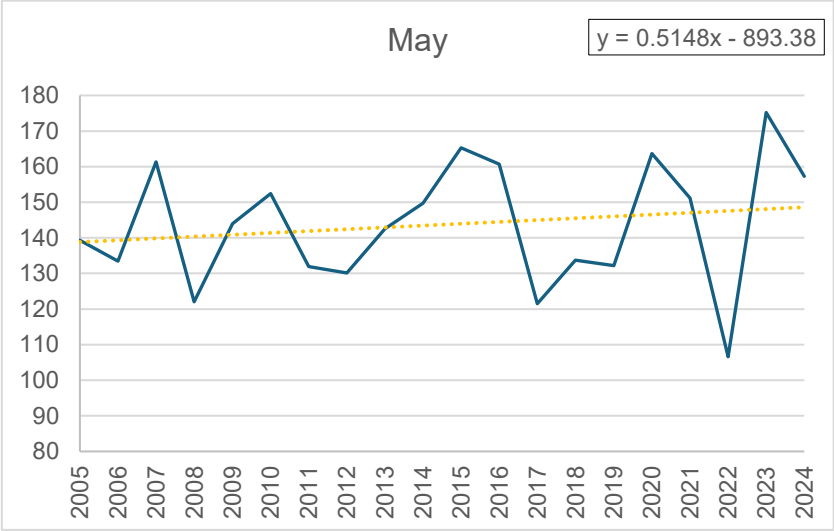


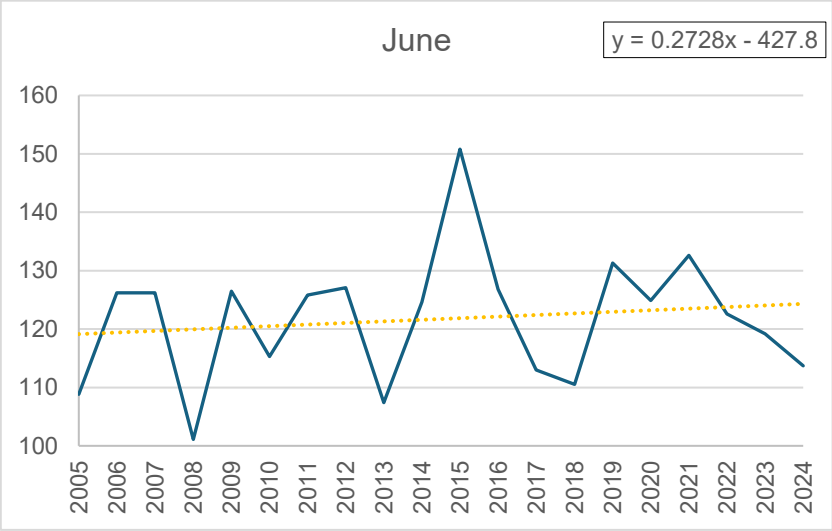


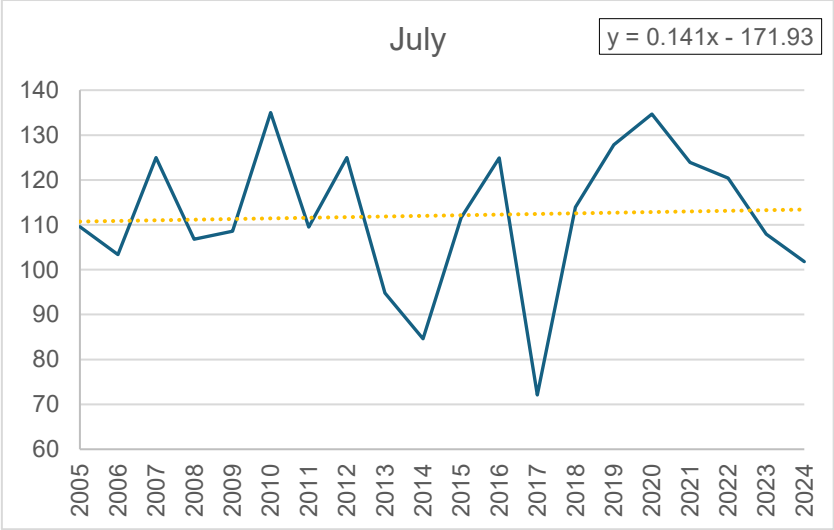


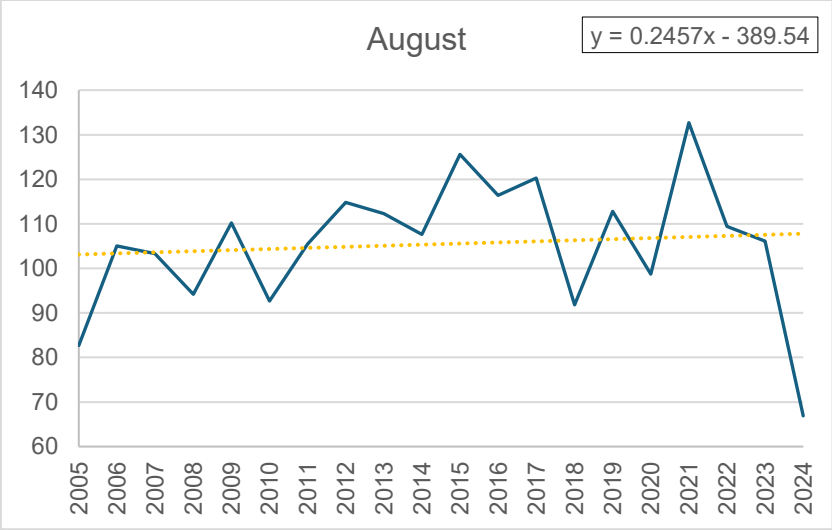

**Appendix B** Monthly evapotranspiration (mm) graph and trendline between 2005 and 2024 (continue).